

**STUDY ON THE CONFORMATION OF COMB-LIKE POLYMERS (CLPs) CONFINED
TO A SOLID SURFACE**

by

Wei Guan

B.S. in Chemical Engineering, University of Tulsa, 2013

Submitted to the Graduate Faculty of
Swanson School of Engineering in partial fulfillment
of the requirements for the degree of
Master of Science

University of Pittsburgh

2015

UNIVERSITY OF PITTSBURGH
SWANSON SCHOOL OF ENGINEERING

This thesis was presented

by

Wei Guan

It was defended on

March 27th, 2015

and approved by

Di Gao, Ph.D., Associate Professor, Department of Chemical and Petroleum Engineering

Ioannis Bourmpakis, Ph.D., Assistant Professor, Department of Chemical and Petroleum Engineering

Thesis Advisor: Lei Li, Ph.D., Assistant Professor, Department of Chemical and Petroleum Engineering

Copyright © by Wei Guan

2015

STUDY ON THE CONFORMATION OF COMB-LIKE POLYMERS (CLPs)

CONFINED TO A SOLID SURFACE

Wei Guan, M.S.

University of Pittsburgh, 2015

Naonometer-thick lubricants, such as perfluoropolyether (PFPE) ZDOL, have been used to protect magnetic media surface from wear damage in hard disk drives (HDD) for several decades. PFPE's salient weaknesses like high cost, environmental concerns, and notable thickness have challenged their future usage in this fast developing industry. In order to identify a good substitute of PFPEs to alleviate those negative effects, as well as decrease the magnetic spacing, the nanofilm conformation of a novel lubricant, called comb-like polymers (CLPs), confined to the silicon wafer surface has been investigated via studying the molecular weight dependence of the monolayer thickness in this thesis. CLP nanofilm was fabricated through dip-coating process. Saturated bonded thickness of CLPs was determined by spectroscopic ellipsometry (SE) and taken as monolayer thickness. Experimental results showed that the monolayer thicknesses of PFPE ZDOL 2000 and PFPE ZDOL 4000 were 1.02 ± 0.11 nm and 1.59 ± 0.21 nm, respectively. The corresponding molecular weight exponent "n" of ZDOL was 0.64 ± 0.06 , which indicates a slightly stretched random coil conformation. The monolayer thicknesses of four different CLPs, commercially known as PF-636, PF-6320, PF-656 and PF-6520, were 0.48 ± 0.02 nm, 0.69 ± 0.05 nm, 0.64 ± 0.04 nm, and 0.80 ± 0.06 nm, respectively, which are significantly lower than that of Zdol. The "n" values of PF-63X and PF-65X were 0.33 ± 0.04 , and 0.20 ± 0.01 , respectively, which indicates a flatter conformation than ZDOL. The difference between PFPEs and CLPs has been attributed to the different rigidity of ZDOL and CLP

molecules caused by different chemical structure of their backbones and side groups. Our experimental results suggest that the CLP chains are more rigid and tend to lie flatter on the silicon wafer surface and it will potentially reduce magnetic spacing and increase the areal density. The experimental results also indicated that the rigidity of the CLP chains result in faster solution adsorption. Though more reliability tests are required to determine the feasibility of CLPs as a media lubricant, the current studies suggest that CLPs have great potential as nanometer-thick lubricant.

TABLE OF CONTENTS

PREFACE.....	XIII
1.0 INTRODUCTION.....	1
1.1 IMPORTANCE OF DISK LUBRICANTS.....	1
1.2 DISADVANTAGES OF THE STATE-OF-THE ART DISK LUBRICANTS 	2
1.3 INNOVATION THAT EXCITES COMB-LIKE POLYMERS (CLPS).....	3
1.4 OBJECTIVE AND APPROACH TO DETERMINE MONOLAYER THICKNESS AND CONFORMATION.....	6
2.0 LITERATURE REVIEW.....	8
2.1 SPREADING.....	8
2.2 SURFACE ENERGY MEASUREMENT.....	10
2.3 TITRATION.....	13
2.4 BEAD DENSITY PROFILE AND RADIUS OF GYRATION CALCULATION.....	14
3.0 METHODOLOGY.....	17
3.1 MATERIALS.....	17
3.2 UV/O₃ CLEANING.....	17
3.3 SAMPLE FABRICATION.....	19

3.4	ELLIPSOMETRY	23
3.5	EXPERIMENTAL PROCEDURE (FOR A COMPLETE CYCLE OF EACH SINGLE MEASUREMENT)	27
4.0	RESULTS	28
4.1	ZDOL 2000 AND ZDOL 4000	28
4.2	PF-636 AND PF-6320	31
4.3	PF-656 AND PF-6520	34
5.0	DISCUSSION	38
5.1	CONFORMATION OF ZDOL	39
5.2	CONFORMATION OF CLPS	46
5.3	ADSORPTION KINETICS	52
6.0	CONCLUSION.....	56
	APPENDIX A.....	58
	BIBLIOGRAPHY.....	63

LIST OF TABLES

Table 1. Material properties of PFPEs and CLPs	4
Table 2. Average radius of gyration and self-diffusion coefficient of ZTMD, Mono, ZDOL and A20H. ¹⁵ (Copyright © 2007, IEEE).....	16
Table 3. Bonded thicknesses of ZDOL 2000.....	28
Table 4. Bonded thicknesses of ZDOL 4000.....	29
Table 5. Monolayer thickness and n value of ZDOL 2000 and ZDOL 4000	31
Table 6. Bonded Thicknesses Results of PF-636.....	32
Table 7. Bonded Thicknesses Results of PF-6320.....	32
Table 8. Material properties of PFPEs and CLPs	34
Table 9. Bonded Thicknesses Results of PF-656.....	35
Table 10. Bonded Thicknesses Results of PF-6520.....	35
Table 11. Monolayer thickness and n value of PF-656 and PF-6520.....	37
Table 12. Results summary of monolayer thickness and n values	38
Table 13. Monolayer thickness and n value of ZDOL determined by various methodologies	40
Table 14. Water contact angle and hexadecane contact angle measurements of PF-636.....	58
Table 15. Water contact angle and hexadecane contact angle measurements of PF-636.....	58
Table 16. Water contact angle and hexadecane contact angle measurements of PF-636.....	59

Table 17. Water contact angle and hexadecane contact angle measurements of PF-636.....	59
Table 18. Water contact angle and hexadecane contact angle measurements of PF-636.....	59
Table 19. Water contact angle and hexadecane contact angle measurements of PF-636.....	60
Table 20. Water contact angle and hexadecane contact angle measurements of PF-636.....	60
Table 21. Water contact angle and hexadecane contact angle measurements of PF-636.....	60
Table 22. Water contact angle and hexadecane contact angle measurements of PF-636.....	61
Table 23. Water contact angle and hexadecane contact angle measurements of PF-636.....	61

LIST OF FIGURES

Figure 1. Structure of the head-media interface.....	1
Figure 2. (a) Molecular and chemical structure of ZDOL (b) Chemical structure of CLPs PF-636/6320 and PF-656/6520.....	3
Figure 3. Hypothesized adsorption conformation of ZDOL and CLPs on a solid substrate	5
Figure 4. Three conditions of molecular conformation and their corresponding molecular weight dependences	7
Figure 5. (a) Magnetic disk employed in spreading method. Red section indicates submerged area, yellow section indicates the lubricant spreading area, and black line shows the spreading axis. (b) Thickness evolution profile obtained from spreading method. ⁹ (Copyright © 2006, IEEE).....	9
Figure 6. Monolayer thickness as a function of molecular weight. ⁹ (Copyright © 2006, IEEE)	10
Figure 7. (a) Polar surface energy profile as a function of lubricant thickness. ¹¹ (Reprinted with permission from Tyndall, G. W.; Waltman, R. J.; Pocker, D. J. <i>Langmuir</i> 1998, 14, 7527. Copyright © 1998, American Chemical Society) (b) Layering structure of ZDOL on magnetic media disk surface. ¹² (Reprinted from <i>Tribology Series</i> ; Vol. Volume 40, B. Marchon, D. Dowson, M. P. G. D., Lubrecht, A. A., Eds.; The physics of boundry lubrication at the head disk interface, p 217. Copyright © 2002, with permission from Elsevier.....	12
Figure 8. ZDOL titration of CHx (circle) and CNx (square) surfaces as a function of ZDOL molecular weight. Solid symbols correspond to the maximum ZDOL thickness	

that can be bonded to the carbon surface while open symbols indicates minima obtained from surface energy measurements.¹¹ (Reprinted with permission from Tyndall, G.W.; Waltman, R.J.; Pocker, D. J. *Langmuir* 1998, 14, 7527. Copyright © 1998, American Chemical Society)..... 13

Figure 9. Bead density profile and typical equilibrium snapshots of (a) ZDOL, (b) Mono, (c) A20H, and (d) ZTMD multilayers.¹⁵ (Copyright © 2007, IEEE)..... 15

Figure 10. Chemical structures and bead-spring model of ZDOL, A20H, Mono, and ZTMD.¹⁵ (Copyright © 2007, IEEE)..... 15

Figure 11. UV/Ozone ProCleaner..... 18

Figure 12. Simplified schematic representation of UV/ozone cleaning process.¹⁸ (Reprinted with permission from Vig, J. In *Surface Contamination*; Mittal, K. L., Ed.; Springer US: 1979, p 235. Copyright © 1985, American Vacuum Society)..... 18

Figure 13. Dip-coater instrument..... 20

Figure 14. Thickness of total (solid line), bonded (dashed line), and mobile layers (dotted line) of ZDOL as a function of time in 8×10^{-4} M solution.¹⁹ (Springer and Tribology letters, 18, 2005, 279, Lubricant layer formation during the dip-coating process: influence of adsorption and viscous flow mechanism, Merzlikine, A.G.; Li, L.; Jones, P.; Hsia, figure (2), Copyright © 2005, with kind permission from Springer Science and Business Media)..... 20

Figure 15. Thickness of total (solid line), bonded (dashed line), and mobile layers (dotted line) of ZDOL as a function of time in 8×10^{-4} M solution. Total and bonded layer thicknesses were measured after 35-mins of dwell time, while mobile layer thickness were measured at 2-5 min dwell times.¹⁹ (Springer and Tribology letter, 18, 2005, 279, Lubricant layer formation during the dip-coating process: influence of adsorption and viscous flow mechanism, Merzlikine, A.G.; Li, L.; Jones, P.; Hsia, figure (6), Copyright © 2005, with kind permission from Springer Science and Business Media)..... 21

Figure 16. Fabrication of lubricant film on solid substrate via dip-coating process.²⁰ (Reprinted with permission from Wang, Y.; Sun, J.; Li, L. *Langmuir* 2012, 28, 6151. Copyright © 2012, American Chemical Society)..... 22

Figure 17. alpha-SE 23

Figure 18. Schematic illustration of a general ellipsometer setup..... 24

Figure 19. Illustration of two-layer film structure on silicon wafer substrate	25
Figure 20. (a) Cauchy layer model parameter specification and (b) ellipsometry fitting result using CompleteEase software	26
Figure 21. Curve fitting result of (a) ZDOL 2000 and (b) ZDOL 4000	30
Figure 22. Curve fitting results of (a) PF-636 and (b) PF-6320	33
Figure 23. Curve fitting results of (a) PF-656 and (b) PF-6520	36
Figure 24. Ideal chain bead model. ²⁵ (Copyright © 1953, Cornell University Press).....	42
Figure 25. Polymer chain conformations in a good, theta, and poor solvent. ²⁶ (Copyright© Robert Thomas).....	45
Figure 26. (a) Torsional potential for the perfluoroethan C-C bond and (b) torsional potential forthe bond. ²⁷ (Springer and Tribology letters, 7, 1999, 91, Impact of polymer structure and confinement on the kinetics of Zdol 4000 bonding to amorphous- hydrogenated carbon, Waltman, R. J.; Tyndall, G. W.; Pacansky, J.; Berry, R. J. figure (6), (7), Copyright © 1999, with kind permission from Springer Science and Business Media).....	47
Figure 27. Schematic description of electron donation mechanism. ¹ (Reprinted with permission from Cornaglia, L.; Gellman, A. J. Journal of Vacuum Science & Technology A 1997, 15, 2755. Copyright © 1997, American Vacuum Society)	50
Figure 28. Schematic ZDOL and CLPs conformation based on current thesis results.....	51
Figure 29. (a) Adsorption prolife of ZDOL as a function of molar concentration (b) Adsorption profile of CLPs as a function of molar concentration. (All experiments are based on 30 min dwell time).....	54
Figure 30. Surface energy profile of PF-636. Black symbols correspond to total surface energy, green symbols correspond to polar surface energy, and red symbols correspond to dispersive surface energy.....	62
Figure 31. Surface energy profile of PF-6320. Black symbols correspond to total surface energy, green symbols correspond to polar surface energy, and red symbols correspond to dispersive surface energy.....	62

PREFACE

The author would like to thank Dr. Lei Li for methodology guidance and valuable discussions. He also appreciates Ph.D candidate Andrew Kozbial for experimental instruments training, software instruction, data analysis, and helpful discussions, appreciate Ph.D candidate Yongjing Wang for technical support, and warmly appreciate Seagate Technology LLC for providing ZDOL.

1.0 INTRODUCTION

1.1 IMPORTANCE OF DISK LUBRICANTS

In hard disk drive (HDD) industry, protecting magnetic media surface from wear damage caused by intermittent read/write head and disk surface contacts during operations is important for producing reliable, durable and successful recording storage products; thus, a hydrogenated amorphous carbon overcoat is introduced to the magnetic media surface, and this carbon overcoat is further protected by an ultra-thin lubricant film to provide dependable protection.¹ The structures of magnetic media, read/write head, and head-media interface are shown in Figure 1. The lubricant layer is nanometer-thick and controlling its properties is important for long-term operation of the HDD.

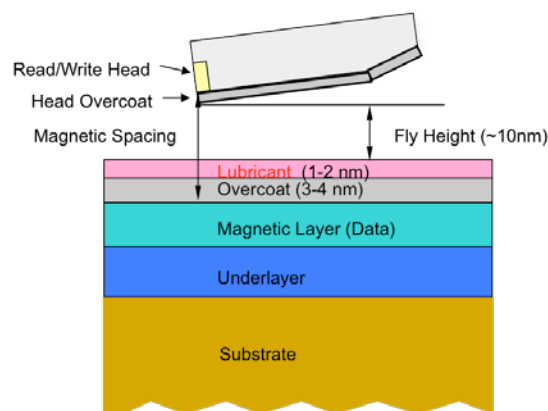


Figure 1. Structure of the head-media interface.

Besides damage protection, the areal density of HDD is another key factor that needs to be considered. Currently, the industrial goal is to exceed 1 Tb/in² areal density, which requires decreasing the magnetic spacing to less than 6.5 nm. Specifically, one design criteria is to allocate 1nm each for disk overcoat, head overcoat, and disk lubricant film, leaving 3.5 nm fly-height for head-disk operation.² However, currently used disk lubricant thickness is greater than 1 nm, therefore, developing new HDD lubricant nanofilms has been a notable research area in magnetic recording industry.

1.2 DISADVANTAGES OF THE STATE-OF-THE ART DISK LUBRICANTS

Currently, perfluoropolyethers (PFPEs) functionalized with hydroxyl polar end groups like Fomblin ZDOL (Figure 2a) are commercially used as disk lubricants due to their good lubricity, high thermal stability, high chemical inertness, low surface energy, and low vapor pressure.³ However, aside from these good properties, they have salient drawbacks such as high price, toxicity and environmental issues. It has been reported that fluorotelomer alcohol (FTOH) can degrade in the atmosphere initiated by OH radical to form perfluorinated carboxylic acid (PFCA), which is a potentially toxic and carcinogenic contaminant that degrades very slowly because there is no metabolic or environmental degradation pathway.⁴ PFCA was also found to accumulate in human and animal tissues collected in local and remote global locations.⁴ Unfortunately, ZDOL is one such kind of FTOH. In addition, it was also found that PFPEs have global warming potential since both C-F and C-O bonds can adsorb thermal radiation between the range from 750 and 1250 cm⁻¹, which is called “atmospheric window”; therefore, these anthropogenic compounds like PFPEs have the ability to block the escape of terrestrial radiation

and cause global warming as a result.⁵ In addition, degradation of PFPEs is catalyzed by the presence of Lewis acids that are commonly found on the disk surface, which makes this problem more severe.^{6,7}

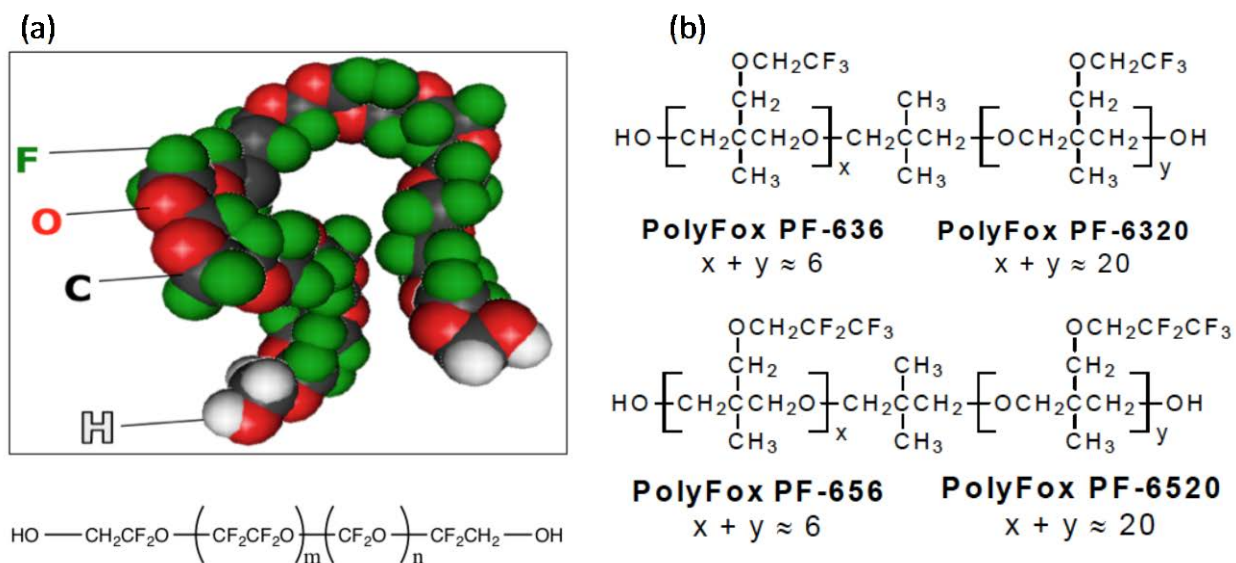


Figure 2. (a) Molecular and chemical structure of ZDOL; (b) Chemical structure of CLPs PF-636/6320 and PF- 656/6520.

1.3 INNOVATION THAT EXCITES COMB-LIKE POLYMERS (CLPS)

By considering the aforementioned weaknesses of currently used disk lubricants, it is critical to develop alternatives to alleviate issues of PFPEs. In this thesis, the nanofilm conformation of the novel disk lubricant called “comb-like polymers”, which have similar material properties compared to PFPEs, (See Table 1) but unique advantages, have been investigated. CLPs have a hydrocarbon backbone instead of a fluorocarbon backbone with one hydroxyl functional group on each end of the main chain. In addition, CLPs are combed with partially fluorinated side chains $-\text{O}-\text{CH}_2-\text{CF}_2-\text{CF}_3$ (PF-656 & PF-6520) and $-\text{O}-\text{CH}_2-\text{CF}_3$ (PF-636 & PF-6320) while

PFPEs are single, flexible perfluoropolyether chains. In the current research, two series of CLPs, commercially known as PF-63X and PF-65X, were studied and their chemical structures are shown in Figure 2b.

Table 1. Material properties of PFPEs and CLPs.

	ZDOL2000	ZDOL4000	PF-636	PF-6320	PF-656	PF-6520
MW (g/mol)	2000	4000	1,150	3,480	1,490	4,480
SG (g/ml)	1.82	1.82	1.20	1.22	1.27	1.31
Viscosity (cps)	182	182	2,300	5,500	1,800	6,000
Surface Tension (mN/m)	22	22	35.5	29.2	30.1	28.0
Refractive Index	1.30	1.30	1.41	1.42	1.39	1.38

The distinct structures of CLPs make them more environmentally friendly and much cheaper than PFPEs. Based on previous study,^{6,8} catalyzed degradation of PFPEs happens at ether bonds located between two CF₂ groups (CF₂-O-CF₂), while CLPs lacks of such structure, therefore, CLPs were expected to have moderately reduced degradation issue during high-temperature operation of hard disk drive. In addition, CLPs is ~80 times less expensive than ZDOL. Most importantly, we postulated CLPs are good substitutes for PFPEs as disk lubricants based on their chemical structures and hypothetical conformations when confined to a solid substrate as shown in Figure 3. ZDOL takes an oblate-like random coil conformation due to the flexibility of ZDOL backbone, while CLPs chains are more rigid, which results in a flatter conformation compared to ZDOL with their combs preferentially oriented towards the air-lubricant interface due to the chemical characteristics of -CF₃. Fluorine atom has the highest electronegativity among all elements, thus it is able to strongly attract electrons and form eight

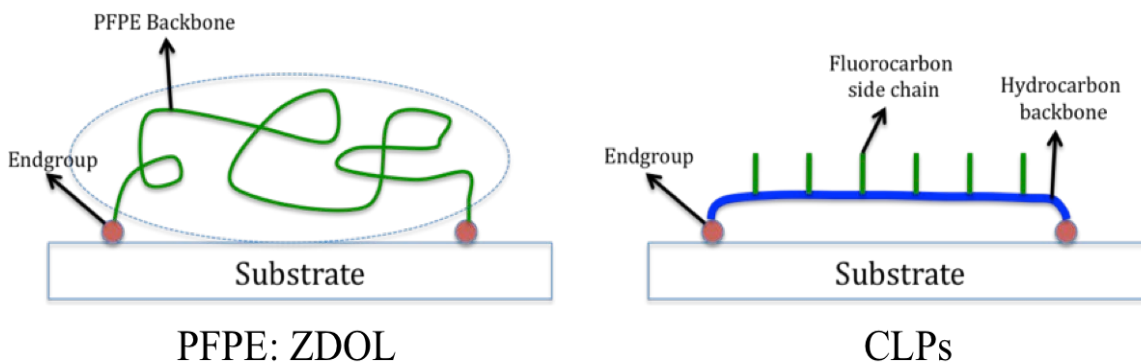


Figure 3. Hypothesized adsorption conformation of ZDOL and CLPs on a solid substrate.

valence electron steady-state like noble gases. This results in the low polarizability and thus low inter-segment Van der Waals force. As a consequence, the surface tension is low. Similar to PFPEs, CLPs have $-\text{CF}_3$ groups in their side chains. Moreover, $-\text{CF}_3$ combs are expected to face towards air-lubricant interface to minimize the surface tension, which will give CLPs the desirable low surface tension and great chemical inertness just like PFPEs. As a result, besides bulky side combs and backbone rigidity effects, the hydrocarbon backbones of CLPs are expected to be pushed downward by side combs to lay flatter on the solid surface than PFPEs. Therefore, CLPs are expected to have lower monolayer thickness and thus reduce the magnetic spacing, which can allow for increased areal density of hard disk drives (HDDs). On account of that, CLPs have great theoretical potential to replace PFPEs as disk lubricants for magnetic recording industry.

1.4 OBJECTIVE AND APPROACH TO DETERMINE MONOLAYER THICKNESS AND CONFORMATION

CLPs have drawn our attention due to their advantages and potentially similar functionality to PFPEs. Among all properties of a disk lubricant, understanding the conformation of the lubricant on the solid surface is critical and attracts interest because it is the foundation of understanding the nanometer-thick lubricant's properties and will further guide the design of the next-generation lubricant in HDD application. Therefore, this thesis focuses on experimentally determining the conformation of CLPs confined to a silicon wafer. In order to elucidate molecular conformation, the molecular weight dependence of the monolayer thickness was studied according to Eq. 1^{9,10}:

$$h_{ML} \propto MW^n \quad Eq.1$$

h_{ML} is the monolayer thickness, MW corresponds to the molecular weight, and “n” is the molecular weight exponent. If the polymer takes an ideal “random coil” conformation; $n=0.5$. If the polymer lays absolutely flat on the substrate, the monolayer thickness is independent of molecular weight and $n=0$. If the polymer stands straight up on the substrate, the monolayer thickness is proportional to molecular weight and $n=1$. (See Figure 4)

As far as this approach is concerned, characterizing the monolayer thickness of adsorbed lubricant film is the critical step as long as polymer molecular weight is known. Since the monolayer thickness of a polymer is within nanometer range, it is difficult to obtain ideally well packed single molecular layer in reality based on current fabrication techniques; therefore, definition of monolayer is still under debate and method of measuring the monolayer thickness varies from researcher to researcher.

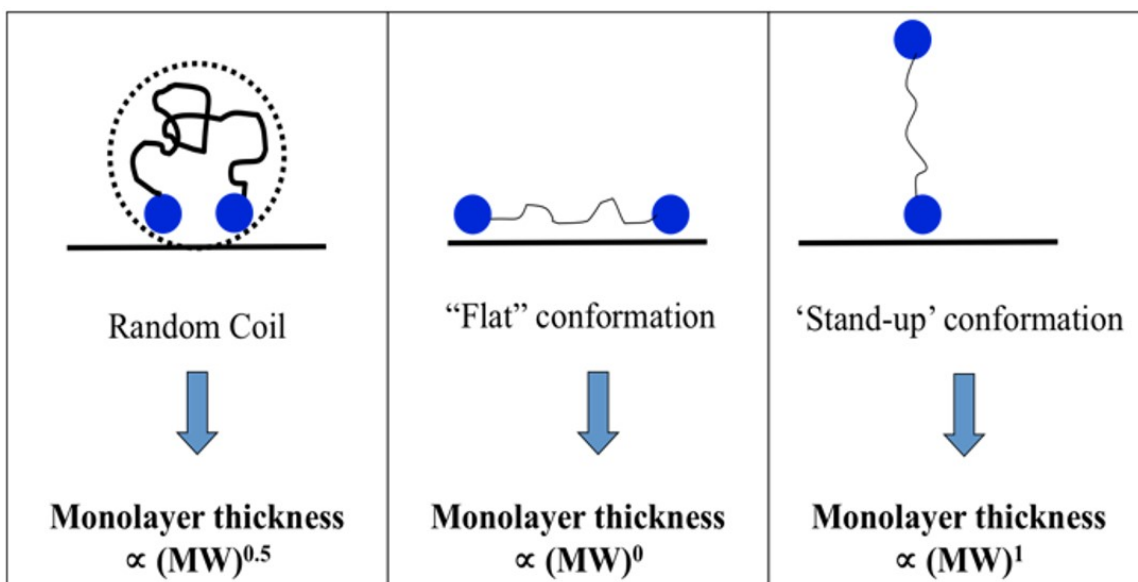


Figure 4. Three conditions of molecular conformation and their corresponding molecular weight dependences.

In this thesis, the monolayer thicknesses of ZDOL and CLPs were defined as the maximum bonded thickness of the polymer that can be adsorbed on the silicon wafer substrate via hydrogen bonding interactions between polar end groups of polymers and the substrate surface polar active sites, and were experimentally determined using ellipsometry (alpha-SE). To achieve this, the lubricant was applied on the silicon wafer substrate by dip-coating process and then washed with a good solvent to remove mobile fraction and obtained the bonded layer only. By increasing the concentration of the lubricant solution, the saturated (maximum) adsorbed bonded thickness was determined and defined as the monolayer thickness. Then conformation of CLPs was studied based on monolayer thicknesses, n value, and kinetics data. Comparisons were made between ZDOL and CLPs.

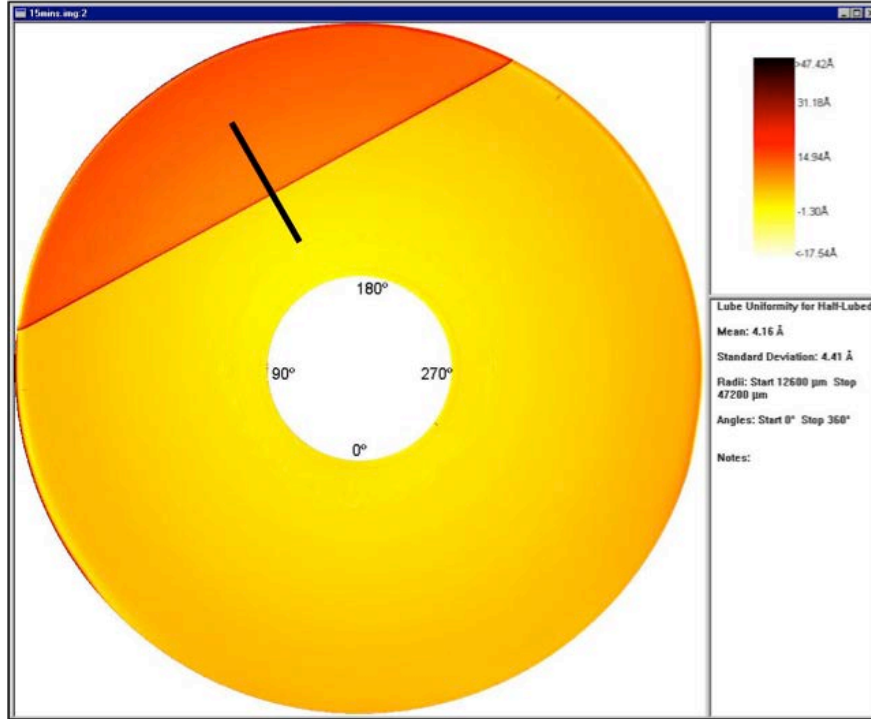
2.0 LITERATURE REVIEW

Previously, great efforts were made to measure the monolayer thickness of nanometer-thick PFPE lubricant film and different techniques have been employed.

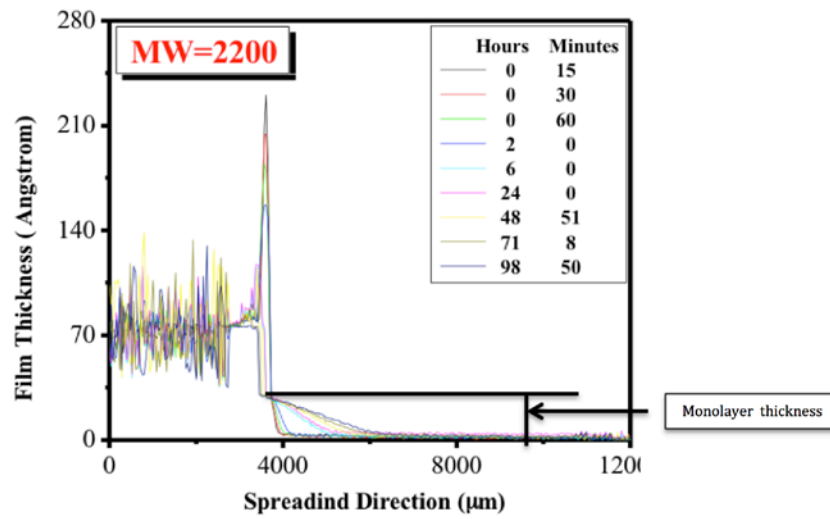
2.1 SPREADING

One technique is spreading as shown in Figure 5a. In this method, the magnetic disk is partially dip-coated with Zdol lubricant, after allowing a certain period of time for lubricant molecules to travel along the spreading axis on the disk surface, a layering structure can be observed. Plotting the thickness as a function of spreading distance using optical surface analyzer (OSA), by varying either initial concentration, or dwell time (the time period during which magnetic disk is totally submerged into lubricant solution), several different flowing curves can be obtained. Interestingly, there will be remarkable step changes of thickness for each curve, and the thickness corresponding to the lowest step change is defined as the monolayer thickness as shown in Figure 5b.

Based on the spreading method, monolayer thicknesses of ZDOL (MW=2200) and of ZDOL (MW=3700) were found to be around 2.3 nm and 2.9 nm, respectively, and a molecular weight exponent (n) of 0.46 was obtained by plotting monolayer thickness versus number



(a)



(b)

Figure 5. (a) Magnetic disk employed in spreading method. Red section indicates submerged area, yellow section indicates the lubricant spreading area, and black line shows the spreading axis. (b) Thickness evolution profile obtained from spreading method.⁹ (Copyright © 2006, IEEE)

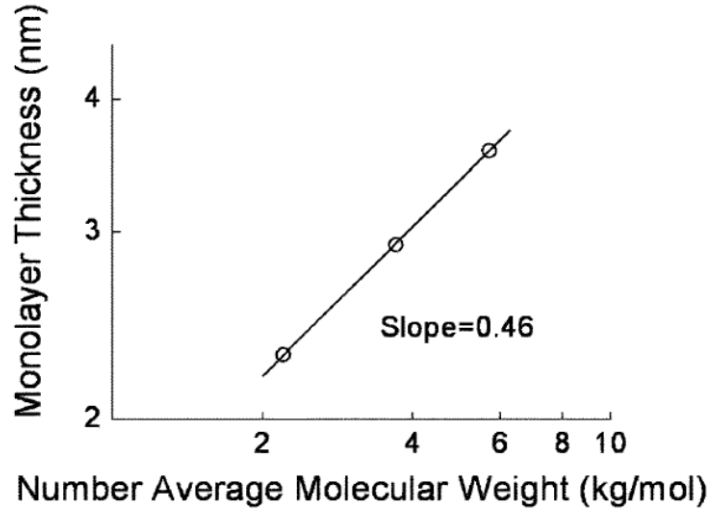


Figure 6. Monolayer thickness as a function of molecular weight.⁹ (Copyright © 2006, IEEE)

average molecular weight (See Figure 6), which indicates a close Gaussian-coil-like behavior for ZDOL, *i.e.*, $h_m \propto M_n^{0.5}$.⁹ Same methodology has also been conducted by Ma *et al.* and an *n* value of 0.6 was reported.¹⁰

2.2 SURFACE ENERGY MEASUREMENT

Surface energy measurement is another methodology previous researchers have used to investigate the monolayer thickness. It has been found that the polar component of surface energy will oscillate as the lubricant thickness increases due to the polymer layering structure. This phenomenon can be explained by using an empirical expression presented as Eq. 2¹¹:

$$\Delta F = \gamma_i + \gamma_j - (\zeta_{jj} + \zeta_{ij}) \quad \text{Eq.2}$$

ΔF is the polar free energy of lubricant, γ_i is the polar surface energy of the substrate, and γ_j is the surface energy of the non-interacting polar end groups of the *j*th lubricant

monolayer. ζ_{jj} was defined as the in-plane, lateral, cohesive interaction energy density between the lubricant molecules in the j th monolayer and ζ_{ij} was the adhesive interaction energy density between the j th lubricant layer and the underlying carbon substrate coated with i monolayers of lubricant.¹¹ By considering that hydroxyl end groups are the only polar part of the polymer while perfluorinated backbone is strongly non-polar, surface energy is strongly dependent on polar end group interactions and interactions between polar end group and the surface active bonding sites.

Within sub-monolayer regime, γ_i is large and constant. As the amount of lubricant bonded to carbon overcoat increases, γ_j and ζ_{jj} decrease since nearly all polar end groups are bonded to the surface due to the existence of adequate active bonding sites on substrate, and ζ_{ij} becomes larger as the amount of polar end groups interacting with carbon substrate increases. Taking all these factors into consideration, with the increase of lubricant thickness, polar surface energy will decrease from bare carbon overcoat surface energy to the surface energy of a carbon substrate fully covered with lubricant monolayer. Beyond the monolayer region, as the amount of lubricants increases, the number of free polar end groups will increase due to limited amount of available bonding sites, which results in an increase of γ_j . ζ_{jj} will also increase however the increasing amount is smaller than γ_j if considering not all free polar end groups will interact with each other. ζ_{ij} remains small; as a result, the total surface energy increases. When the amount of lubricant added exceeds two monolayers, ζ_{ij} and ζ_{jj} increase dramatically and become dominant factors, which will cause the total surface energy to drop back. All in all, if considering the fact that interactions between polar end groups of lubricant and active bonding sites of substrate is stronger than cohesive and adhesive interactions between end groups, the minimum polar surface energy occurs when the first monolayer is formed or full coverage of lubricants on surface is fulfilled as shown in Figure 7.^{11,12}

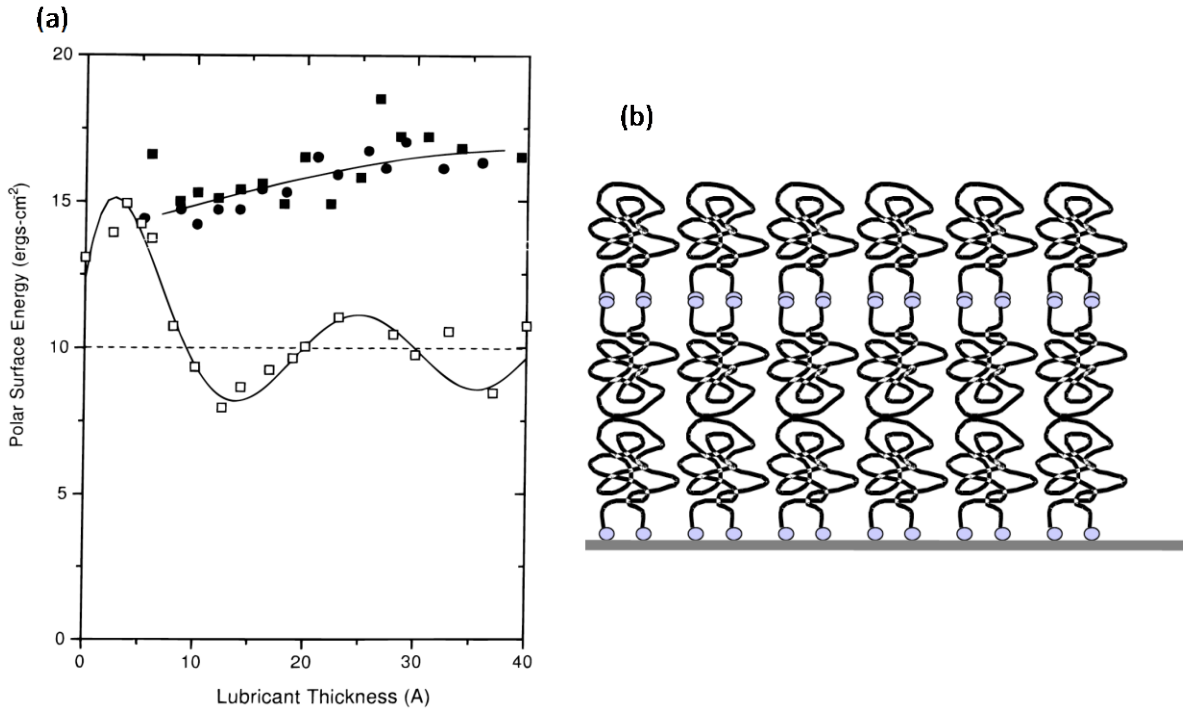


Figure 7. (a) Polar surface energy profile as a function of lubricant thickness.¹¹ (a) Polar surface energy profile as a function of lubricant thickness.¹¹ (Reprinted with permission from Tyndall, G. W.; Waltman, R. J.; Pocker, D. J. *Langmuir* 1998,14, 7527. Copyright © 1998, American Chemical Society) (b) Layering structure of ZDOL on magnetic media disk surface.¹² (Reprinted from *Tribology Series*; Vol. Volume 40, B. Marchon, D. Dowson, M. P. G. D., Lubrecht, A. A., Eds.; *The physics of boundry lubrication at the head disk interface*, p 217. Copyright © 2002, with permission from Elsevier)

Thus, monolayer thickness can be determined via surface energy measurement by exploring the lubricant thickness corresponds to the first minimum polar surface energy in the polar surface energy evolution profile. Based on Tyndall's results, monolayer thickness of ZDOL 2000 and ZDOL 4000 on carbon overcoat is 1.4 ± 0.1 (nm) and 2.5 ± 0.2 (nm), respectively, which is slightly different from Guo *et al.*'s results.^{9,11} However, reasons need to be further investigated.

2.3 TITRATION

In addition to surface energy, Tyndall also employed a titration method by annealing an excessive amount of lubricant onto the disk surface until thickness plateaus in order to explore the monolayer thickness. The obtained thickness corresponds to the maximum amount of lubricant that can bond onto the surface and is defined as the monolayer thickness.¹¹

The results of surface energy and annealing methods taken on two different carbon surfaces are shown in Figure 8. As shown, both surface energy method and titration method gave similar monolayer thickness values according to Tyndall¹¹. More importantly, based on Tyndall's results¹¹, monolayer thickness increases linearly with polymer molecular weight, which means the n value is close to 1.0 and indicates a “stand-up” film conformation. Compared to Guo's $n=0.46$ conclusion, the difference is significant.^{9,11} Guo *et al.* also explored molecular weight dependence via surface energy measurements and obtained a molecular weight exponent of 0.51,¹³ which is close to her spreading results but different from Tyndall's finding.

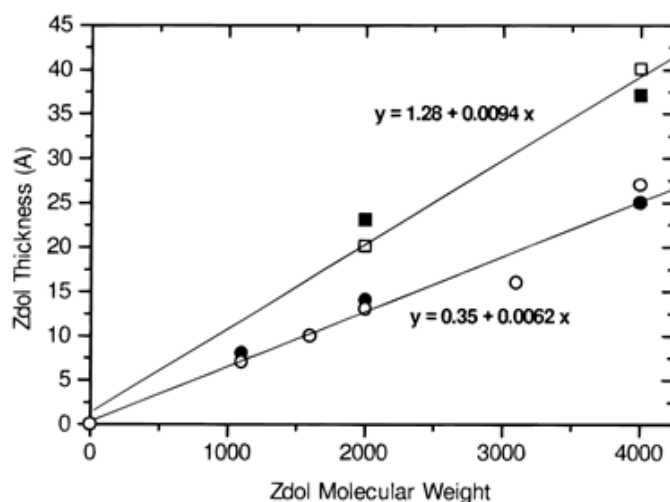


Figure 8. ZDOL titration of CHx (circle) and CNx (square) surfaces as a function of ZDOL molecular weight. Solid symbols correspond to the maximum ZDOL thickness that can be bonded to the carbon surface while open symbols indicates minima obtained from surface energy measurements.¹¹ (Reprinted with permission from Tyndall, G.W.; Waltman, R.J.; Pocker, D. J. *Langmuir* 1998, 14, 7527. Copyright © 1998, American Chemical Society)

It is hard to explain why the same methodology gave rise to significant differences in results; one possible reason could be different treatments to the original substrate surface, which can lead to differences in chemical compositions of substrate surfaces, thus change the interaction between substrate and polymers as a result.^{11,14} Another contribution might be the technique employed in monolayer thickness measurement. In Guo's research⁹, all film thickness measurements were taken by optical surface analyzer (OSA) while Tyndall used Fourier Transform Infrared Spectroscopy (FTIR) to measurement film thickness.¹¹ However, systematic investigation is necessary to further uncover all the possible contributors.

2.4 BEAD DENSITY PROFILE AND RADIUS OF GYRATION CALCULATION

In addition to measuring monolayer thickness to elucidate molecular conformation, previous researchers have also used bead density profiles (See Figure 9) to investigate layering structures and have used mathematical model (Eq. 3) to calculate radius of gyration in order to investigate conformations of PFPEs with different molecular structures.¹⁵ (See structures in Figure 10)

$$R_g^2 = \frac{1}{N_m} \sum_{i=1}^{N_m} [(x_i - x_g)^2 + (y_i - y_g)^2 + (z_i - z_g)^2] = 2R_{gxy}^2 + R_{gz}^2 \quad \text{Eq.3}$$

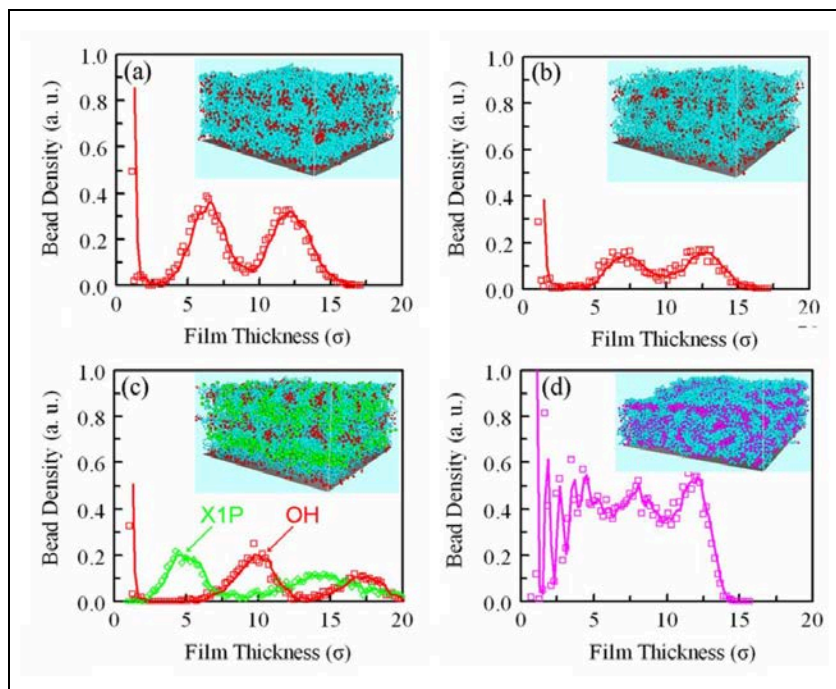


Figure 9. Bead density profile and typical equilibrium snapshots of (a) ZDOL, (b) Mono, (c) A20H, and (d) ZTMD multilayers.¹⁵ (Copyright © 2007, IEEE)

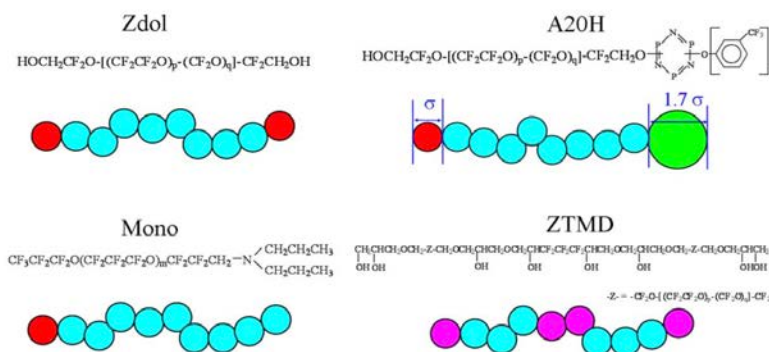


Figure 10. Chemical structures and bead-spring model of ZDOL, A20H, Mono, and ZTMD.¹⁵ (Copyright © 2007, IEEE)

In the bead density profile of ZDOL, the distance between two adjacent peaks is believed to be two monolayers, which also indicates a layering structure with polar end groups bonded to the substrate within monolayer regime and clustered together at the interface of two layers beyond monolayer regime as the surface energy results suggested before (see Figure 7b).

Radius of gyration results are listed in Table 2. Since the R_{gxy} of all PFPEs are larger than R_{gzy} , this suggests a slightly flat conformation for PFPE monolayer. This conclusion is close to Guo's results⁹, however, it is inconsistent with Tyndall's finding.¹¹ The slightly flat conformation of PFPE's is also substantiated in work by Karplus *et al.*¹⁶ and Mayeed and Kato,¹⁷ which attributed the flattening to the polar ether groups in PFPE backbone.

Table 2. Average radius of gyration and self-diffusion coefficient of ZTMD, Mono, ZDOL and A20H.¹⁵

(Copyright © 2007, IEEE)

Lubricants	$R_{gxy}(\sigma)$	$R_{gzy}(\sigma)$	$D (\times 10^{-4} \sigma^2/\tau)$
ZTMD	0.79	0.59	2.5
Mono	0.86	0.69	46
Zdol	0.78	0.71	32
A20H	0.84	0.81	27

3.0 METHODOLOGY

3.1 MATERIALS

Fomblin ZDOL 2000 and ZDOL 4000 were obtained from Solvay Solexis Inc. and used as received. Polyfox CLPs PF-636, PF-6320, PF-656, and PF-6520 were obtained from Omnova Solutions and used as received. Chemical structures of the PFPE and CLP lubricant polymers are shown before in Figure 2 and selected properties are presented in Table 1. The suffixes of CLPs indicate the total number of repeating units: *e.g.*, there are six repeating units and twenty repeating units in 636 and 6320, respectively. 2,3-Dihydrodecafluoropentane (DuPont Vertrel-XF) was used as solvent for PFPEs and CLPs and used as received. SiO₂ wafers with native oxide were purchased from Silicon Quest International, Inc. (P/B<100> 1-10 OHM-CM 279±25 μm) and used as lubricant substrate.

3.2 UV/O₃ CLEANING

UV Ozone Cleaner purchased from BioForce Nanosciences, Inc. was used to clean hydrocarbon contaminants on the surface of bare silicon wafer (see Figure 11) and cleaning mechanism of O₃ and UV radiation is shown in Figure 12.

energy required to dissociate O₂ into two ground state oxygen atoms, which will further generate oxygen, is 245.4 nm; however, just below 245.4 nm the dissociation is very weak, a good wavelength of dissociating O₂ and producing O₃ is 184.9 nm.¹⁸ This process corresponds to the lower step in Figure 12. Meanwhile, most hydrocarbons have strong adsorption between 200 nm and 300 nm, therefore, the wavelength of 253.7 nm generated by low- pressure mercury discharge tube is very useful in exciting and dissociating those hydrocarbon contaminants. Moreover, the adsorption of O₃ reaches maximum near 253.7 nm. Therefore, with the existence of both wavelengths, O₃ will continually be formed and destroyed, and an intermediate product during both formation and destruction process is atomic oxygen, which is a strong oxidizing agent that can react with those dissociated hydrocarbon contaminants and form volatile products like CO₂, H₂O, N₂, etc. to achieve the cleaning purpose.¹⁸

3.3 SAMPLE FABRICATION

Fabrication of lubricant film onto SiO₂ was achieved by dipcoater purchased from KSV Instruments via dip-coating process (See Figure 13). During dip-coating, two different mechanisms, adsorption and viscous flow, are responsible for the formation of nanometer-thick lubricant film, which consists of two different lubricant regimes called mobile and bonded fraction. This process has been experimentally proven by Merzlikine *et al.*¹⁹ and his findings are summarized below in Figure 14 and Figure 15.



Figure 13. Dip-coater instrument

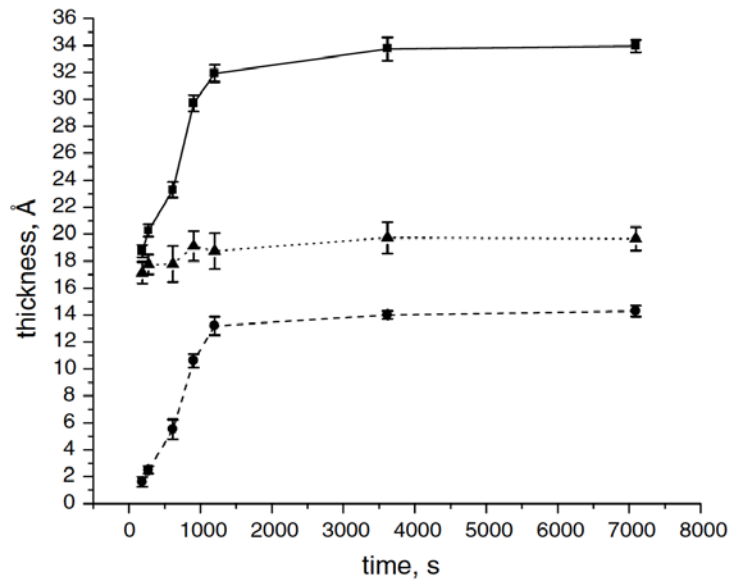


Figure 14. Thickness of total (solid line), bonded (dashed line), and mobile layers (dotted line) of ZDOL as a function of time in 8×10^{-4} M solution.¹⁹ (Springer and Tribology letter, 18, 2005, 279, Lubricant layer formation during the dip-coating process: influence of adsorption and viscous flow mechanism, Merzlikine, A.G.; Li, L.; Jones, P.; Hsia, figure (2), Copyright © 2005, with kind permission from Springer Science and Business Media)

Based on Figure 14, it is clear that dwell time is responsible for the formation of bonded layer via adsorption mechanism since mobile layer is independent of the dwell time and the

thickness of the bonded layer increases with the dwell time. An empirical equation corresponding to this mechanism has been proposed by Merzlikine *et al.*¹⁹ As shown in Eq. 4, where y is the bonded thickness, x represents concentration, and y_0 , A_0 , and x_0 are three constants:

$$y = y_0 + A_0 \left(1 - e^{-\frac{x}{x_0}} \right) \quad \text{Eq.4}$$

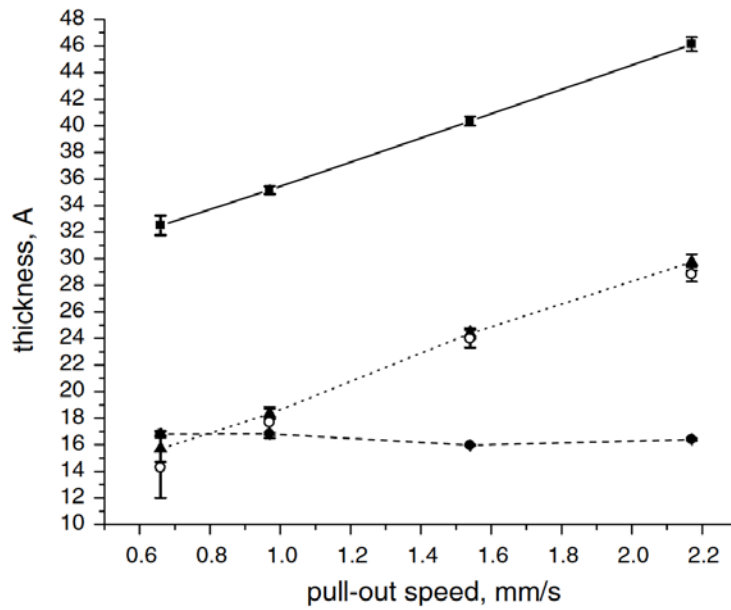


Figure 15. Thickness of total (solid line), bonded (dashed line), and mobile layers (dotted line) of ZDOL as a function of time in 8×10^{-4} M solution. Total and bonded layer thicknesses were measured after 35-mins of dwell time, while mobile layer thicknesses were measured at 2-5 min dwell times.¹⁹ (Springer and Tribology letter, 18, 2005, 279, Lubricant layer formation during the dip-coating process: influence of adsorption and viscous flow mechanism, Merzlikine, A.G.; Li, L.; Jones, P.; Hsia, figure (6), Copyright © 2005, with kind permission from Springer Science and Business Media

Figure 15 indicates how pull-out speed affects the formation of mobile layer through viscous flow mechanism, as pull-out speed increases, mobile layer thickness increases almost linearly. This result can be described by Eq. 5:¹⁹

$$h_0 = 0.93(\mu v)^{\frac{2}{3}} \sigma^{-\frac{1}{6}} (\rho g)^{-\frac{1}{2}} \quad \text{Eq.5}$$

where h_0 is the mobile layer thickness, μ is the solution viscosity, v is the pull-out speed, σ is the solution surface tension, and ρ is the solution density. The surface adsorption and viscous flow mechanisms were further illustrated by Wang *et al.* and are shown in Figure 16.²⁰

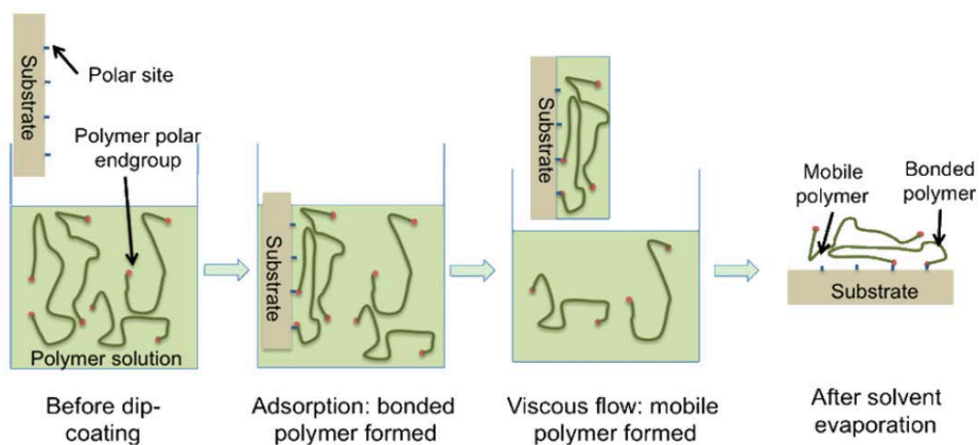


Figure 16. Fabrication of lubricant film on solid substrate via dip-coating process.²⁰ (Reprinted with permission from Wang, Y.; Sun, J.; Li, L. *Langmuir* 2012, 28, 6151. Copyright © 2012, American Chemical Society)

As Figure 16 shows, the bonded layer is formed via hydrogen-bonding interactions between polar end groups of polymers and active surface bonding sites through adsorption process;⁷ however, there is no such interaction established between end groups of mobile polymers and the surface active bonding sites; thus they easily flow on the surface and named as “mobile”. But they are still pulled out along with those bonded polymers via viscous flow mechanism. Since the mobile layer has no hydrogen-bonding interaction with substrate, they can be easily washed away by a good solvent, which gives us the fundamental theoretical support of the methodology employed in the washing process of this thesis.

3.4 ELLIPSOMETRY

Thickness measurements were taken by an alpha-SE obtained from J.A. Woollam Co. (see Figure 17).



Figure 17. alpha-SE.

Interior structure schematic was shown in Figure 18. As shown the core facilities making up ellipsometry includes a light beam which provides a monochromatic light source, a polarizer that produces linearly polarized incident light, a compensator as a super achromatic retarder controlled by a computer, a sample stage which holds the sample, an analyzer whose azimuth angle is variable and controlled by software, and a detector that can measure the amplitude and phase difference between two orthogonal electric field components of emergent light, which were notated as Ψ and ϕ , respectively.²¹

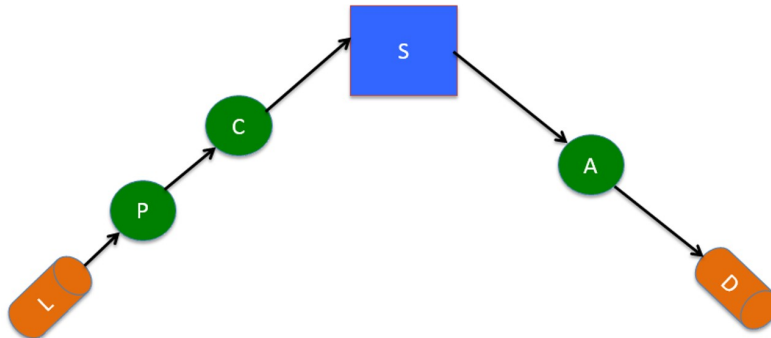


Figure 18. Schematic illustration of a general ellipsometer setup.

During measurements, a two-layer model was used to determine the thickness of lubricant film. (See Figure 19) The native oxide thickness was measured using a native oxide model and the lubricant layer was modeled by the Cauchy dispersion model. Cauchy-layer model (Eq. 7)

$$n(\lambda) = A + \frac{B}{\lambda^2} \quad \text{Eq.7}$$

is used because it assumes the polymer adsorption coefficient (k) to be zero which correlates well to the polymers being studied due to the ultra-thin feature and clearness of polymer film.²²

A and B are two optical constants which were specified during data analyzing (See Figure 20a) and the wavelength (λ) is a known testing parameter.

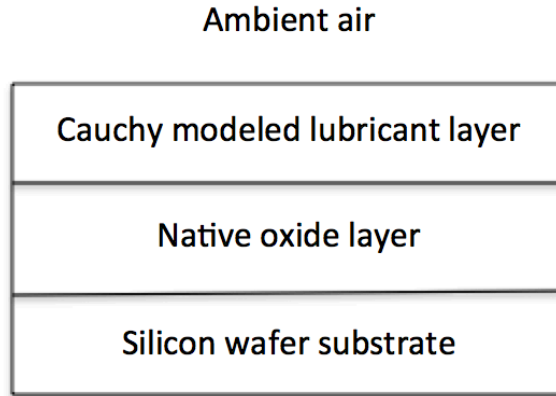


Figure 19. Illustration of two-layer film structure on silicon wafer substrate.

Thus, everything on the right side of Eq. 7 is known; on the left side is the refractive index, which is a function of wavelength, however, it is also a function of sample film thickness. The relation between refractive index and film thickness is built through complex math, which will not be discussed here, and detailed derivation process can be found in Jung *et al.*'s decent work on ellipsometry background.²¹

If experimentally measured Ψ and ϕ data versus wavelength λ were fitted using Eq. 7, by changing film thickness on the left side, the best fitting which gives the smallest mean square error can be achieved at a certain film thickness, and that thickness is the ellipsometry measured thickness of lubricant film. See a fitting sample in Figure 20b.

Layer Commands: **Add Delete Save**

Include Surface Roughness = **OFF**

- Layer # 2 = Cauchy -ZDOL (A=1.30) Thickness # 2 = 0.99 nm (fit) A = 1.300 B = 0.01000 C = 0.00000 k Amplitude = 0.00000 Exponent = 1.500 Band Edge = 400.0 nm
Layer # 1 = NTVE_JAW Native Oxide = 1.29 nm
Substrate = SI_JAW

Angle Offset = **0.030** (fit)

+ **MODEL** Options

+ **FIT** Options

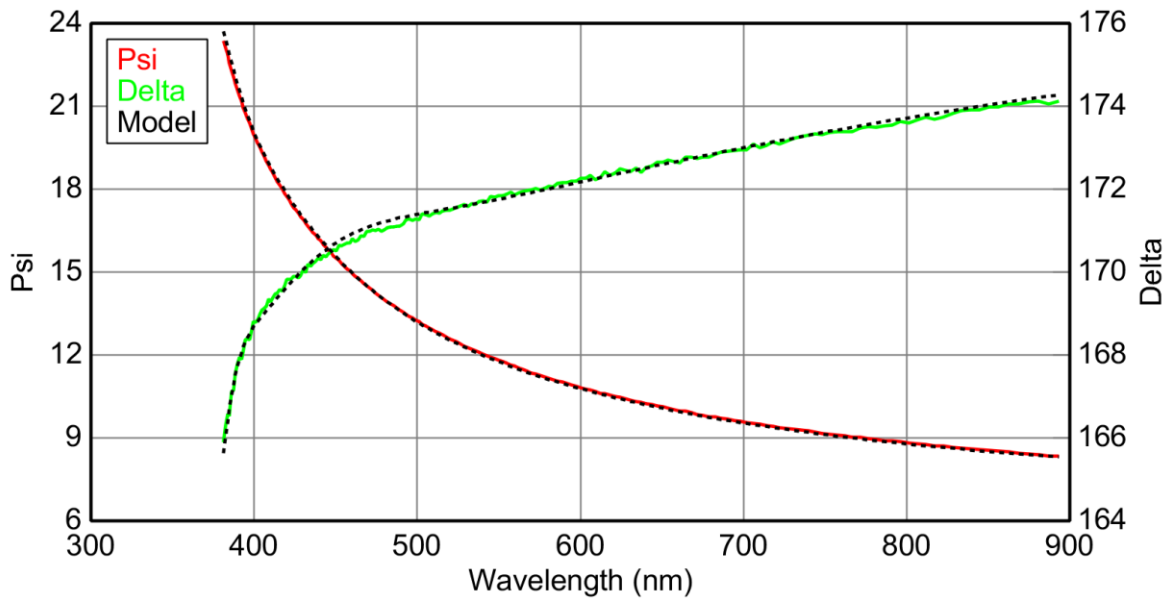
+ **OTHER** Options

Configure Options

Turn Off All Fit Parameters

(a)

Spectroscopic Ellipsometric (SE) Data



(b)

Figure 20. (a) Cauchy layer model parameter specification; (b) ellipsometry fitting result using CompleteEase software.

3.5 EXPERIMENTAL PROCEDURE (FOR A COMPLETE CYCLE OF EACH SINGLE MEASUREMENT)

First, polymer solution was made by weighing appropriate amount of polymer using analytical balance and mixing with a corresponding volume of solvent using graduate cylinder. The solution was well mixed using CDMR for 10 minutes. After the solution was prepared, SiO₂ wafer was cut into suitable size and UV/O₃ treated for 10 minutes to remove contaminants. Afterwards, the native oxide thickness was measured by ellipsometry and fabrication of lubricant film was conducted using dipcoater. During fabrication, 0 min dwell and 30 min dwell were used for PF-63X series and ZDOL/PF-65X series, respectively, and moving speed of dipcoater was set to 60 mm/min. As mentioned previously, the total fabricated lubricant layer consists of two sub-layers called bonded and mobile. The total lubricant thickness was measured using ellipsometry, followed by a washing step to remove the mobile fraction using Vertrel-XF solvent. In this step, everything is the same as fabrication step except using Vertrel-XF solvent instead of polymer solution. Lastly, bonded thickness was measured after washing.

4.0 RESULTS

4.1 ZDOL 2000 AND ZDOL 4000

Bonded layer thickness of ZDOL 2000 measured by ellipsometry is presented in Table 3 and thickness of ZDOL 4000 is presented in Table 4.

Table 3. Bonded thicknesses of ZDOL 2000.

Concentration (g/L)	Bonded Thickness* (nm)					
	Run #1	Run #2	Run #3	Run #4	Average	Std
0.001	0.08	0.06	0.07	0.03	0.06	0.02
0.01	0.16	0.11	0.09	0.10	0.12	0.03
0.1	0.36	0.32	0.25	0.24	0.29	0.06
0.2	0.62	0.35	0.25	0.42	0.41	0.16
0.4	0.81	0.72	0.93	0.57	0.76	0.15
0.8	0.88	0.81	0.93	0.58	0.80	0.15
1.6	0.97	0.86	0.96	0.68	0.87	0.13
3.2	1.27	0.91	0.96	0.92	1.02	0.17
6.4	1.22	1.03	1.07	1.03	1.09	0.09

*Each bonded thickness shown in this table is an average of three individual measurements taken at three randomly picked spots on sample surface; dip-coating process is on a 30 minutes basis.

Table 4. Bonded thicknesses of ZDOL 4000.

Concentration (g/L)	Bonded Thickness* (nm)				
	Run #1	Run #2	Run #3	Average	Std
0.2	0.63	0.45	0.58	0.55	0.09
0.4	0.59	0.53	0.72	0.61	0.10
0.8	0.71	0.77	0.88	0.79	0.09
1.6	0.91	0.97	0.96	0.95	0.03
3.2	1.19	1.22	1.16	1.19	0.03
6.4	1.56	1.38	1.47	1.47	0.09

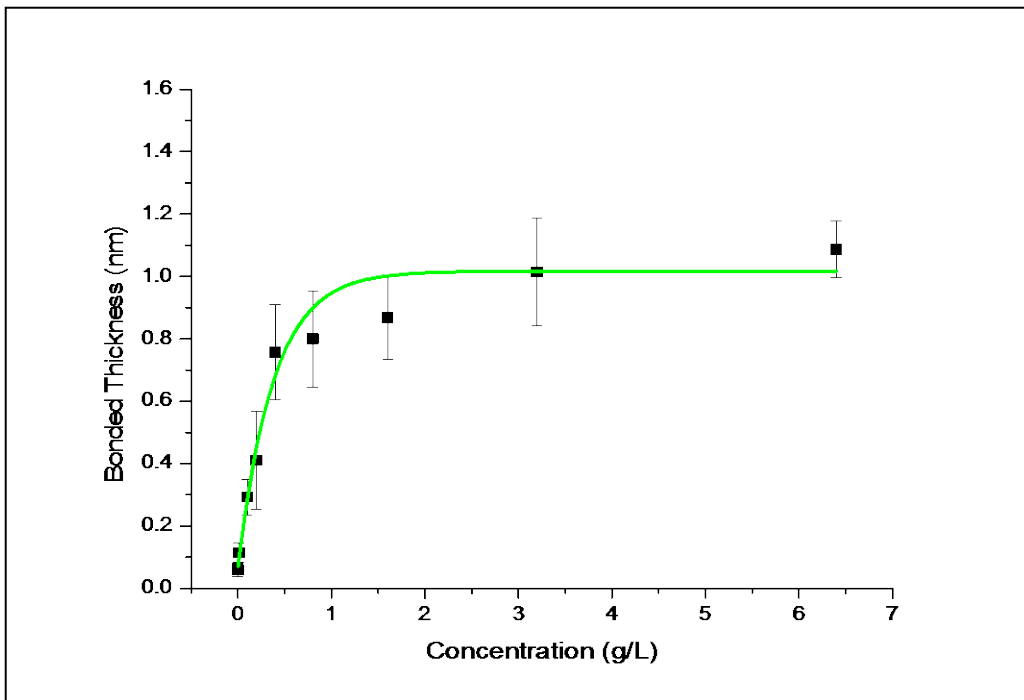
*Each bonded thickness shown in this table is an average of three individual measurements taken at three randomly picked spots on sample surface; dip-coating process is on a 30 minutes basis.

Based on the values shown in Table 3 and Table 4, a functional relationship can be obtained by plotting bonded thickness against concentration. The relationship follows Eq. 4. When concentration approaches infinite, the maximum value of y is reached, and it is equals to y_0+A_0 , which physically means maximum possible amount of polymer is adsorbed onto the substrate; therefore, the corresponding y value is numerically equal to the value of the monolayer thickness. On account of that, as long as the functional relationship can be elucidated using curve fitting, the monolayer thickness can be determined. Curve fitting was done using Origin software, and the fitting results are demonstrated in Figure 21.

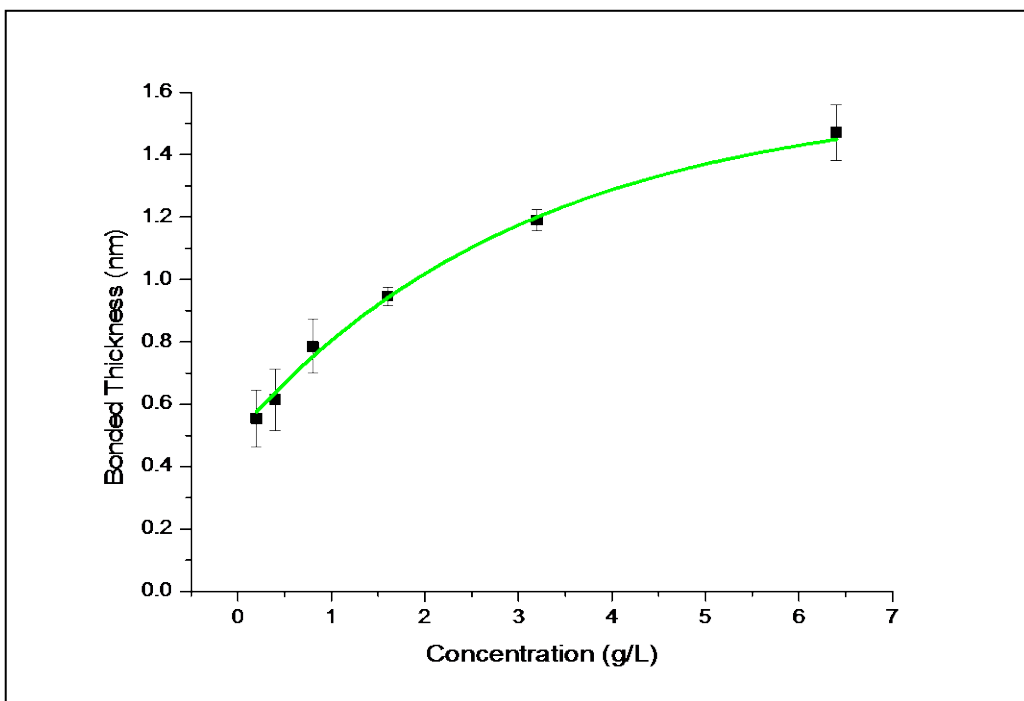
Obtained functional relationships are presented below as Eq. 8 (ZDOL 2000) and Eq. 9 (ZDOL 4000):

$$y = 0.06843 + 0.94845 \left(1 - e^{\left(-\frac{x}{0.38359} \right)} \right) \quad \text{Eq. 8}$$

$$y = 0.50952 + 1.07945 \left(1 - e^{\left(-\frac{x}{3.13621} \right)} \right) \quad \text{Eq. 9}$$



(a)



(b)

Figure 21. Curve fitting result of (a) ZDOL 2000 and (b) ZDOL 4000.

Based on these two equations, the monolayer thickness was determined. Then, n value can be calculated based on Eq. 1. By taking logarithm on each side of Eq. 1, subtracting, and rearranging, a new expression can be obtained (Eq. 10)

$$n = \frac{\ln\left(\frac{H_{ML1}}{H_{ML2}}\right)}{\ln\left(\frac{MW_1}{MW_2}\right)} \quad \text{Eq. 10}$$

The n value can be calculated from Eq. 10 by substituting the measured monolayer thicknesses and molecular weights of ZDOL 2000 and ZDOL 4000 Monolayer thickness results and n value of ZDOL 2000 and ZDOL 4000 are listed in Table 5.

Table 5. Monolayer thickness and n value of ZDOL 2000 and ZDOL 4000.

Polymer	Monolayer Thickness (nm)	n value
ZDOL2000	1.02±0.11	0.64±0.06
ZDOL4000	1.59±0.21	

4.2 PF-636 AND PF-6320

Bonded thickness of PF-636 and PF-6320 are shown in Table 6 and Table 7, respectively. Curve fitting results of PF-636 and PF6320 are shown in Figure 22.

Table 6. Bonded Thicknesses Results of PF-636.

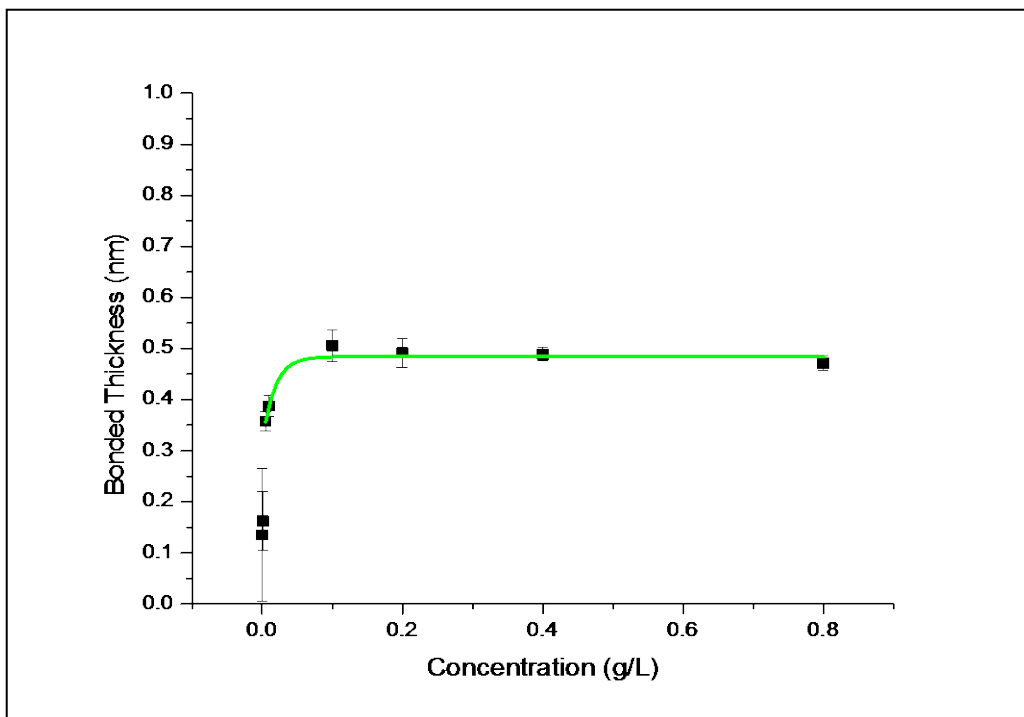
Concentrations (g/L)	Bonded Thickness* (nm)						
	Run #1	Run #2	Run #3	Run #4	Run #5	Average	Std
0.0001	0.25	0.30	0.09	0.02	0.02	0.13	0.13
0.001	0.21	0.24	0.14	0.11	0.12	0.16	0.06
0.005	0.34	0.37	0.37	0.33	0.37	0.36	0.02
0.01	0.38	0.36	0.42	0.38	0.40	0.39	0.02
0.1	0.50	0.50	0.56	0.49	0.47	0.51	0.03
0.2	0.47	0.47	0.54	0.49	0.50	0.49	0.03
0.4	0.47	0.49	0.50	0.48	0.50	0.49	0.01
0.8	0.46	0.46	0.50	0.46	0.47	0.47	0.02

*Each bonded thickness shown in this table is an average of three individual measurements taken at three randomly picked spots on sample surface; dip-coating process is on a 0 minutes basis.

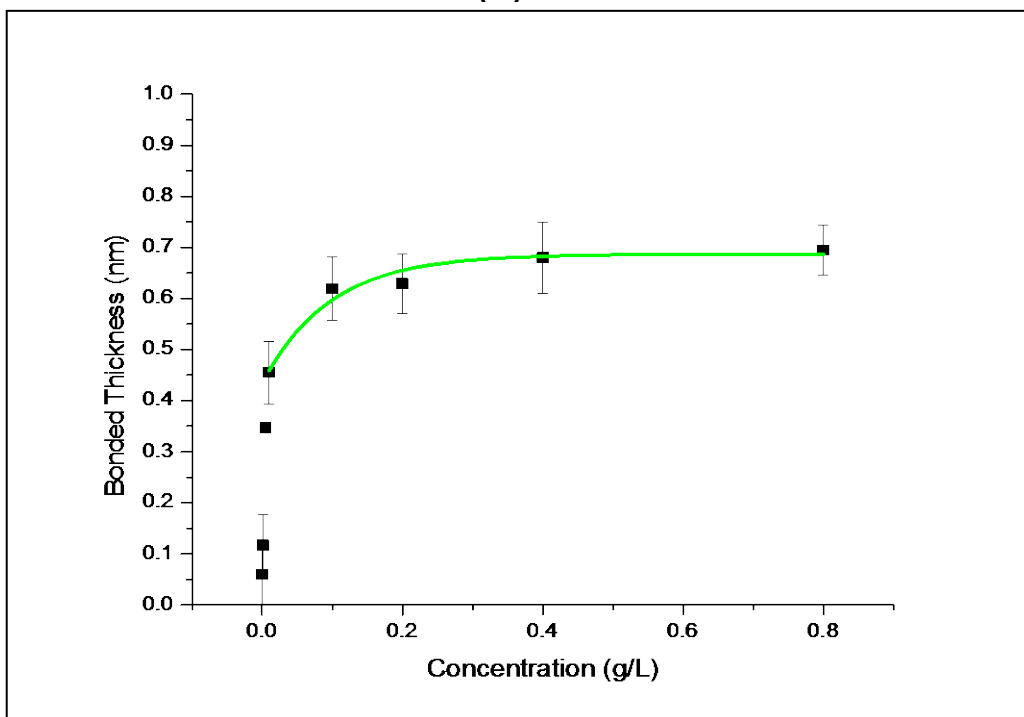
Table 7. Bonded Thicknesses Results of PF-6320.

Concentrations (g/L)	Bonded Thickness* (nm)						
	Run #1	Run #2	Run #3	Run #4	Run #5	Average	Std
0.0001	0.02	0.01	0.12	0.13	0.02	0.06	0.06
0.001	0.07	0.07	0.16	0.20	0.08	0.12	0.06
0.005	0.35	0.35	0.34	0.35	0.35	0.35	0.00
0.01	0.52	0.52	0.43	0.41	0.39	0.45	0.06
0.1	0.67	0.66	0.66	0.55	0.56	0.62	0.06
0.2	0.69	0.60	0.69	0.59	0.57	0.63	0.06
0.4	0.73	0.75	0.72	0.62	0.59	0.68	0.07
0.8	0.73	0.73	0.73	0.64	0.64	0.69	0.05

*Each bonded thickness shown in this table is an average of three individual measurements taken at three randomly picked spots on sample surface; dip-coating process is on a 0 minutes basis.



(a)



(b)

Figure 22. Curve fitting results of (a) PF-636 and (b) PF-6320.

The resulting functional relationships obtained from curve fitting are listed below in Eq. 11 (PF-636) and Eq. 12 (PF-6320):

$$y = 0.18517 + 0.29811 \left(1 - e^{\left(\frac{x}{0.00709} \right)} \right) \quad \text{Eq. 11}$$

$$y = 0.43434 + 0.25211 \left(1 - e^{\left(\frac{x}{0.09635} \right)} \right) \quad \text{Eq. 12}$$

Therefore, monolayer thickness and n value can be calculated as before, and results are presented in Table 8.

Table 8. Material properties of PFPEs and CLPs.

Polymer	Monolayer Thickness (nm)	n value
PF-636	0.48±0.02	0.33±0.04
PF-6320	0.69±0.05	

4.3 PF-656 AND PF-6520

Bonded thickness of PF-656 and PF-6520 taken by ellipsometry are listed in Table 9 and Table 10, respectively. Curve fitting profiles of PF-656 and PF-6520 are shown in Figure 23.

Table 9. Bonded Thicknesses Results of PF-656.

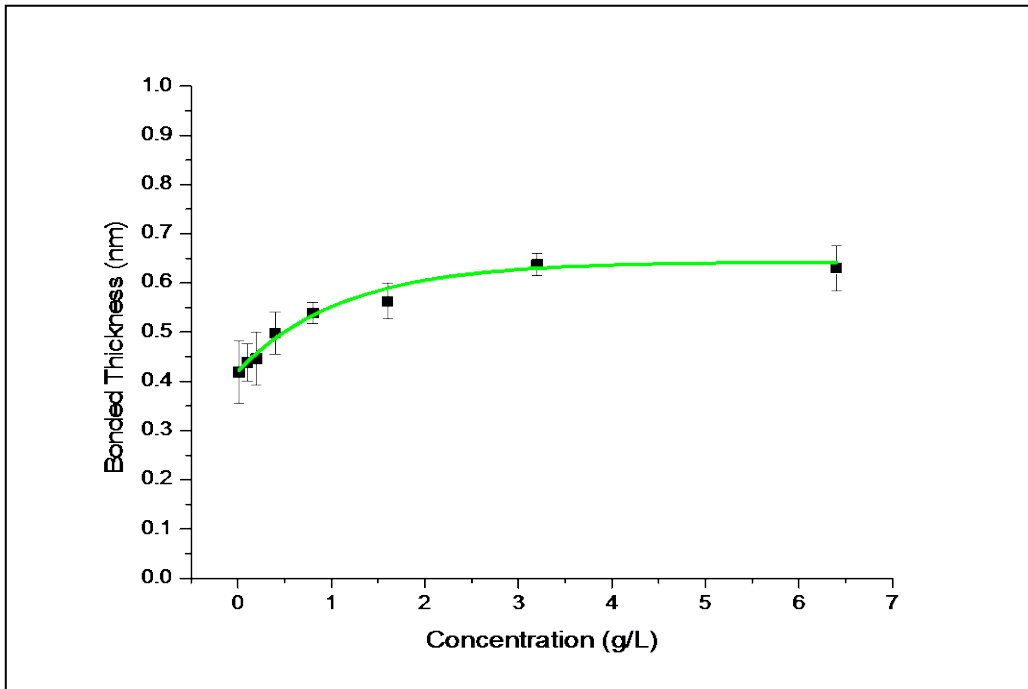
Concentrations (g/L)	Bonded Thickness* (nm)							
	Run#1	Run#2	Run#3	Run#4	Run#5	Run#6	Average	Std
0.01	0.30	0.47	0.40	0.44	0.43	0.47	0.42	0.06
0.1	0.48	0.39	0.44	0.48	0.40	0.44	0.44	0.04
0.2	0.49	0.53	0.42	0.42	0.44	0.38	0.45	0.05
0.4	0.53	0.56	0.46	0.50	0.45	0.48	0.50	0.04
0.8	0.57	0.56	0.54	0.51	0.52	0.54	0.54	0.02
1.6	0.57	0.60	0.60	0.52	0.57	0.52	0.56	0.04
3.2	0.67	0.63	0.65	0.63	0.63	0.61	0.64	0.02
6.4	0.54	0.64	0.67	0.63	0.63	0.67	0.63	0.05

*Each bonded thickness shown in this table is an average of three individual measurements taken at three randomly picked spots on sample surface; dip-coating process is on a 30 minutes basis.

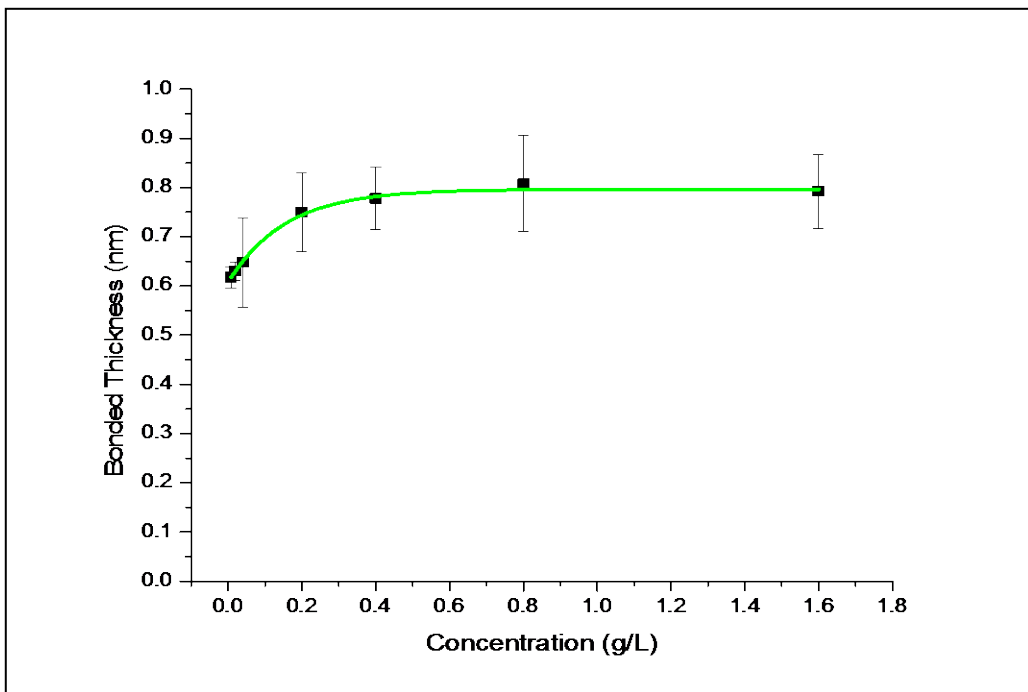
Table 10. Bonded Thicknesses Results of PF-6520.

Concentrations (g/L)	Bonded Thickness* (nm)						
	Run #1	Run #2	Run #3	Run #4	Run #5	Average	Std
0.0016	0.57	0.54	0.54	0.56	0.53	0.55	0.02
0.008	0.59	0.63	0.63	0.64	0.60	0.62	0.02
0.02	0.62	0.65	0.61	0.65	0.62	0.63	0.02
0.04	0.67	0.51	0.73	0.72	0.61	0.65	0.09
0.2	0.66	0.79	0.67	0.79	0.84	0.75	0.08
0.4	0.84	0.78	0.69	0.80	0.83	0.78	0.06
0.8	0.93	0.77	0.70	0.83	0.83	0.81	0.10
1.6	0.89	0.76	0.69	0.79	0.83	0.79	0.07

*Each bonded thickness shown in this table is an average of three individual measurements taken at three randomly picked spots on sample surface; dip-coating process is on a 30 minutes basis.



(a)



(b)

Figure 23. Curve fitting results of (a) PF-656 and (b) PF-6520.

The resulting functional relationships obtained from curve fitting are listed below in Eq. 13 (PF-656) and Eq. 14 (PF-6520):

$$y = 0.42098 + 0.22181 \left(1 - e^{\left(\frac{x}{1.12392} \right)} \right) \quad \text{Eq. 13}$$

$$y = 0.60727 + 0.19472 \left(1 - e^{\left(\frac{x}{0.15585} \right)} \right) \quad \text{Eq. 14}$$

Monolayer thicknesses and n value are presented in Table 11.

Table 11. Monolayer thickness and n value of PF-656 and PF-6520.

Polymer	Monolayer Thickness (nm)	n value
PF-656	0.64±0.04	0.20±0.01
PF-6520	0.80±0.06	

5.0 DISCUSSION

In order to better understand the results, the monolayer thickness of all polymers that have been explored and corresponding “n” values are summarized in Table 12.

Table 12. Results summary of monolayer thickness and n values.

Polymers	Monolayer thickness (nm)	n value
ZDOL2000	1.02±0.11	0.64±0.06
ZDOL4000	1.59±0.21	
PF-636	0.48±0.02	0.33±0.04
PF-6320	0.69±0.05	
PF-656	0.64±0.04	0.20±0.01
PF-6520	0.80±0.06	

5.1 CONFORMATION OF ZDOL

Based on the experimental method used, the obtained monolayer thicknesses of ZDOL 2000 and ZDOL 4000 are 1.02 ± 0.11 nm and 1.59 ± 0.21 nm, respectively. These values should be compared to Tyndall *et al.*'s finding based on surface energy measurement and titration, which indicated the monolayer thickness of ZDOL 2000 and ZDOL 4000 are 1.4 ± 0.1 nm and 2.5 ± 0.2 nm, respectively.¹¹ Our results are significantly smaller. However, the difference is explainable if considering the differences between their measured ZDOL thickness and our measured ZDOL thickness. As mentioned before, the thickness we measured is only bonded layer thickness, while their measured thickness is the total thickness consisting of both bonded and mobile layer since they didn't use any treatment to remove the non-bonded mobile layer that had been fabricated along with bonded layer onto substrate via viscous flow mechanism as discussed before. This can be further supported by Guo's results obtained via spreading method, which reported total monolayer thicknesses of around 2.3 nm for ZDOL 2200 and about 2.9 nm for ZDOL 3700, respectively,⁹ which is even larger than Tyndall's reported values.¹¹ Though, the materials Guo⁹ used are not exactly ZDOL 2000 and ZDOL 4000, but they are close enough to be compared and results are valuable for argument. Another factor that might give rise to the results difference of monolayer thickness measurements might be the different methodologies being used. For convenience, monolayer thickness results and n values based on different methodologies are summarized below in Table 13.

Table 13. Monolayer thickness and n value of ZDOL determined by various methodologies.

Methodology	Polymers	Monolayer thickness (nm)	n values
Saturated bonding adsorption	ZDOL 2000	1.02±0.01	0.64±0.06
	ZDOL 4000	1.59±0.21	
Surface Energy ¹¹	ZDOL 2000	1.4±0.1	1.00
	ZDOL 4000	2.5±0.2	
Surface energy ^{9,13}	N/A	N/A	0.51
Spreading ⁹	ZDOL 2200	2.3	0.46
	ZDOL 3700	2.9	
Spreading ¹⁰	N/A	N/A	0.60

From Table 13, besides different thicknesses being measured, we can clearly see the methodology effect on monolayer thickness determination if you compare surface energy results with spreading results, both of which measured the total thickness, and even based on the same methodology, different researchers have reported different n values. It is also reasonable to postulate that as long as the definition of monolayer thickness is not standardized, and ways of measurement is not generalized, it is very likely to get more different monolayer thicknesses and n values of a same polymer obtained through new methodologies come up with by researchers later on. Other effect like different treatments to origin disk surface can also contribute to a difference in monolayer thickness measurement,^{11,14} but they will not be discussed here in details.

Besides monolayer thicknesses, n values which give direct insight to conformation of polymer thin film is of most interest. Not surprisingly, the n value is also methodology dependent as shown in Table 13. But, our n value of ZDOL, which equals to 0.64±0.06, is basically consistent with results obtained from most previous studies based on different methodologies except for Tyndall's surface energy methodology, which resulted in an n value of

around 1.0. As mentioned before in Table 5, an n value of 1.0 suggests an extremely rigid chain conformation that stands straight up on the solid surface. Reasons behind it are still obscure and needs further investigation. However, most of the reported n values of ZDOL are close to 0.5 or 0.6, which have been confirmed to be the molecular weight dependence of a single flexible ideal polymer chain/bulk polymers or real chains in good solvent.²³ For an ideal chain, the mean square end-to-end distance satisfies the relationship presented below in Eq. 15:

$$\langle r^2 \rangle = N \times a^2 = R_0^2 \quad \text{Eq. 15}$$

where \mathbf{r} is the end to end vector of a single flexible chain, N is the number of random steps needs to be taken to get from one end to the other, \mathbf{a} is a vector of length a with numerous possible orientations. Eq. 15 can be obtained through simple math starting from Equation 16:

$$\mathbf{r} = \mathbf{a}_1 + \mathbf{a}_2 + \dots + \mathbf{a}_N = \sum_{n=1}^N \mathbf{a}_n \quad \text{Eq. 16}$$

This equation can be simplified using a model shown in Figure 24. Each black circle corresponds to a vector \mathbf{a}_N , assume \mathbf{a}_N has only four orientations to take in the next step, which are up, down, left and right in stead of completely independent orientations, then Eq. 17 was obtained;

$$\langle r^2 \rangle = \sum_{nm} \langle \mathbf{a}_n \cdot \mathbf{a}_m \rangle = \sum_n \langle \mathbf{a}_n^2 \rangle = N a^2 = R_0^2 \quad \text{Eq. 17}$$

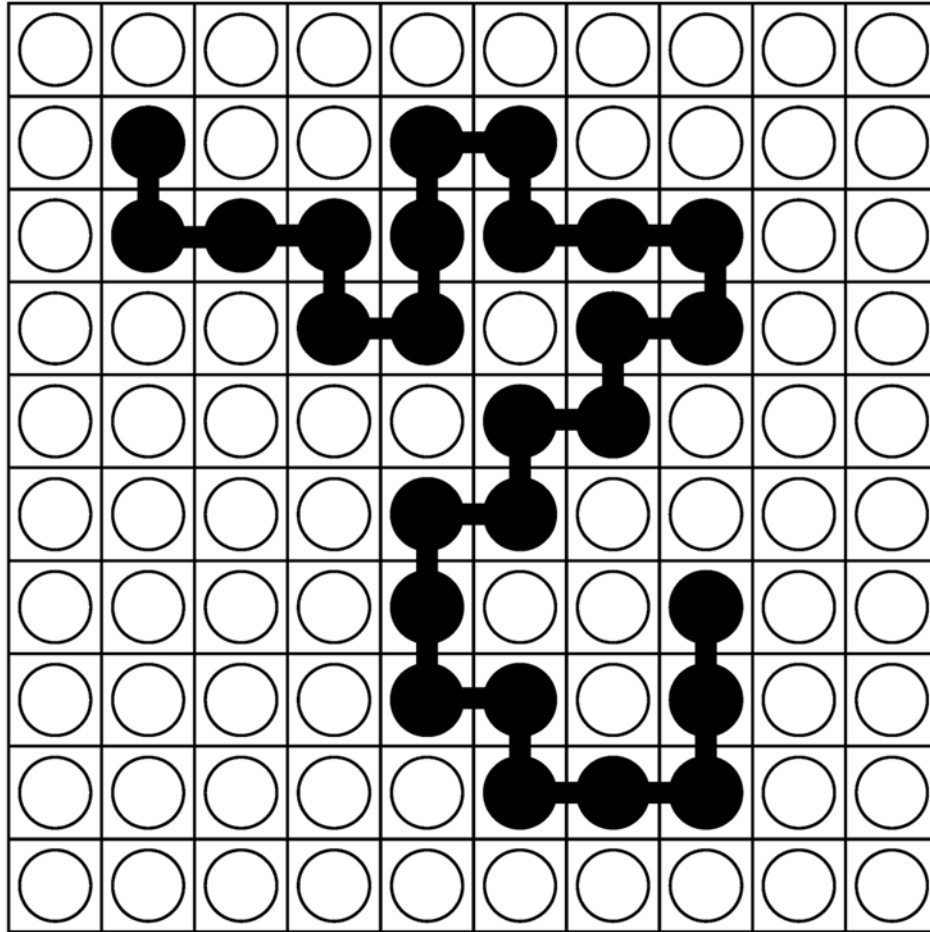


Figure 24. Ideal chain bead model.²⁵ (Copyright © 1953, Cornell University Press)

This is because \mathbf{a}_n and \mathbf{a}_m are either orthogonal or parallel; if they were orthogonal, then $\mathbf{a}_n \cdot \mathbf{a}_m$ is zero; and when they are parallel, $\mathbf{a}_n \cdot \mathbf{a}_m$ equals to a^2 . If Eq. 17 holds, then we can get Eq. 18 by taking square root of the last two terms in Eq. 17.

$$R_0 = a \cdot N^{\frac{1}{2}} \text{ Eq.18}$$

Since N is the number of steps a vector take from one end to another end, thus, it is equal to the number of atoms in a single chain, which is proportional to the molecular weight of a polymer, and the size of a single flexible chain R_0 determines the monolayer thickness h_m .

Therefore, we can rewrite Eq. 18 in the form of molecular weight dependence of monolayer thickness, which is Eq. 1 where n is 0.5 for a single flexible idea chain. More general models have been used for idea chains, which will not be discussed here.

For an ideal chain, the molecular weight exponent n has been proved to be 0.5; so what's the molecular weight exponent n for real chains in good solvent? Many models have been built to calculate n value for real chains in good solvent, and it has been proved to be 0.6, which is slightly large than n of an ideal chain.²³ Flory has proposed a brilliant scheme for n value, which predicts values for all dimensionalities, as shown below.²⁵ Let's start from a single chain with certain unknown radius R and an internal monomer concentration C_{int} . They satisfy a relationship of Eq. 19: (N is total number of monomers in this case, superscript d indicates the dimensionality of the system)

$$C_{int} \cong \frac{N}{R^d} \quad \text{Eq. 19}$$

There is certain repulsive energy in the chain due to monomer-monomer interactions, and it is proportional to number of monomer pairs, thus repulsive energy per unit can be expressed as Eq. 20:

$$F_{resp} = \frac{1}{2} T v(T) C_{int}^2 \quad \text{Eq. 20}$$

One thing to notice is that in Eq. 20, local monolayer concentration C was substituted by C_{int} based on a mean field approach; v is called excluded volume parameter. Integrating Eq. 20 over a volume R^d will give rise to Eq. 21:

$$F_{resp/total} \cong T v(T) C_{int}^2 R^d = T v \frac{N^2}{R^d} \quad \text{Eq. 21}$$

Flory also derived an elastic energy term from idea chain results, which is shown in Eq. 22:

$$F_{el} \cong T \frac{R^2}{N\alpha^2} \quad \text{Eq. 22}$$

Add Eq. 21 and Eq. 22 results in Eq. 23, which is an expression of total energy within a single chain.

$$\frac{F}{T} = \nu \frac{N^2}{R^d} + \frac{R^2}{N\alpha^2} \quad \text{Eq. 23}$$

Total energy has a minimum value when the two terms on right side of the equation is equal to each other, if neglecting all numerical coefficients, we can get Eq. 24:

$$R_F^{d+2} = \nu\alpha^2 N^3 \quad \text{Eq. 24}$$

From there, we can get an important conclusion below:

$$\nu = \frac{3}{d+2} \quad \text{Eq. 25}$$

Based on Eq. 25, it is clearly to see molecular weight exponent ν is 0.6 when d equals to 3 (three dimensional system), which correlates well to real chains in good solvent.²³

In conclusion, based on Flory's model, our calculated ν value result of ZDOL is very close to the result of real chains in good solvent. In other words, the conformation of ZDOL on SiO₂ after solution adsorption using a good solvent under our experimental condition is similar to the conformation of ZDOL in a good solvent before adsorption. Therefore, based on our experimental results, polymer-substrate interactions didn't affect polymer conformation to a significant level that could otherwise be observed. Compared to an ideal chain conformation, a molecular weight exponent of 0.6 indicates a slightly stretched conformation.

Generally speaking, bulk polymer conformation corresponds to ideal chain conformation, under which the only interactions involved are inter-molecular interactions and interactions between segments within a long chain. In addition, under theta solvent condition (a solvent condition which corresponds to a molecular weight exponent of 0.5), the intermolecular and inter-segmental interactions are “equal” to the interactions between polymer molecules/segments and solvent molecules, thus theta condition is equivalent to bulk polymer. While in a good solvent, chains are slightly stretched and give rise to n value of 0.6, which is mainly resulted from the interactions between chain segments and solvent molecules. In a good solvent, from a microscopic point of view, chain segments “like” solvent molecules more than their neighbor segments, thus they will push neighbor segments away from themselves and try to reach an ideal condition that each segment is completely separated by solvent molecules, which macroscopically results in a stretched molecule (see Figure 25).

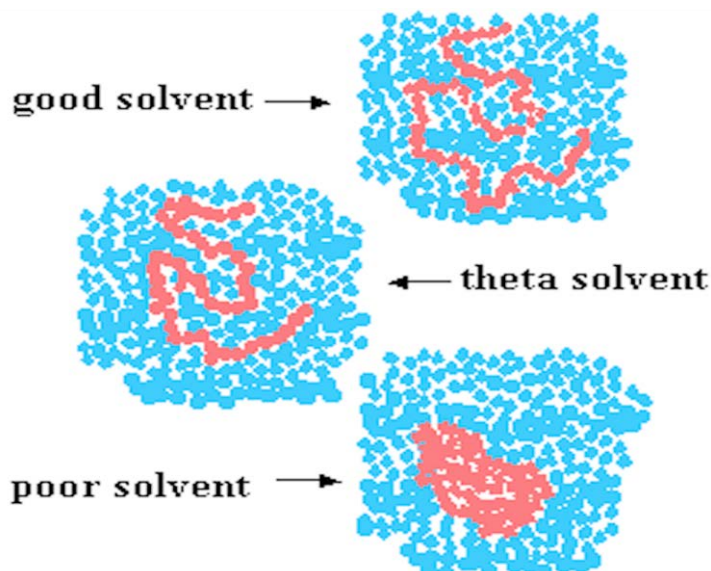


Figure 25. Polymer chain conformations in a good, theta, and poor solvent.²⁶ (Copyright © Robert Thomas)

Back to our results again, since the n value we got is 0.64 ± 0.6 , which is close to 0.6, we hypothesize that the overall interaction involved at the interface of polymer and substrate is not strong enough to affect the conformation. However, the underlying mechanisms need to be further investigated.

5.2 CONFORMATION OF CLPS

As shown before in Table 12, n values of PF-63X and PF-65X are 0.33 ± 0.04 and 0.20 ± 0.01 respectively, which indicate a much flatter conformation compared to ZDOL. Two main reasons may result in the difference of n values between ZDOL and CLPs. The first reason is rotational energy barrier of C-C and C-O single bonds in backbones. As shown in Figure 2, both of ZDOL and CLP backbones are consisted of a series of C-C and C-O bonds, and the ratio of C-O bond to C-C bond is roughly 2:1 in ZDOL backbone, while the ratio in CLP backbone is 1:2. Considering the fact that total repeating units of ZDOL and CLPs with similar molecular weight are about the same, thus, that ratio still holds when total number of bonds is considered. In addition, the rotational energy barrier of C-C bond is generally larger than that of C-O. In terms of that, Waltman *et al.* have done excellent work previously to calculate rotational energy barriers of C-C bond and C-O bond in ZDOL backbone using computational method, and the reported energy barrier of C-C bond and C-O bond are 3.94 kcal/mol and approximately 1kcal/mol, respectively.²⁷ (See Figure 26)

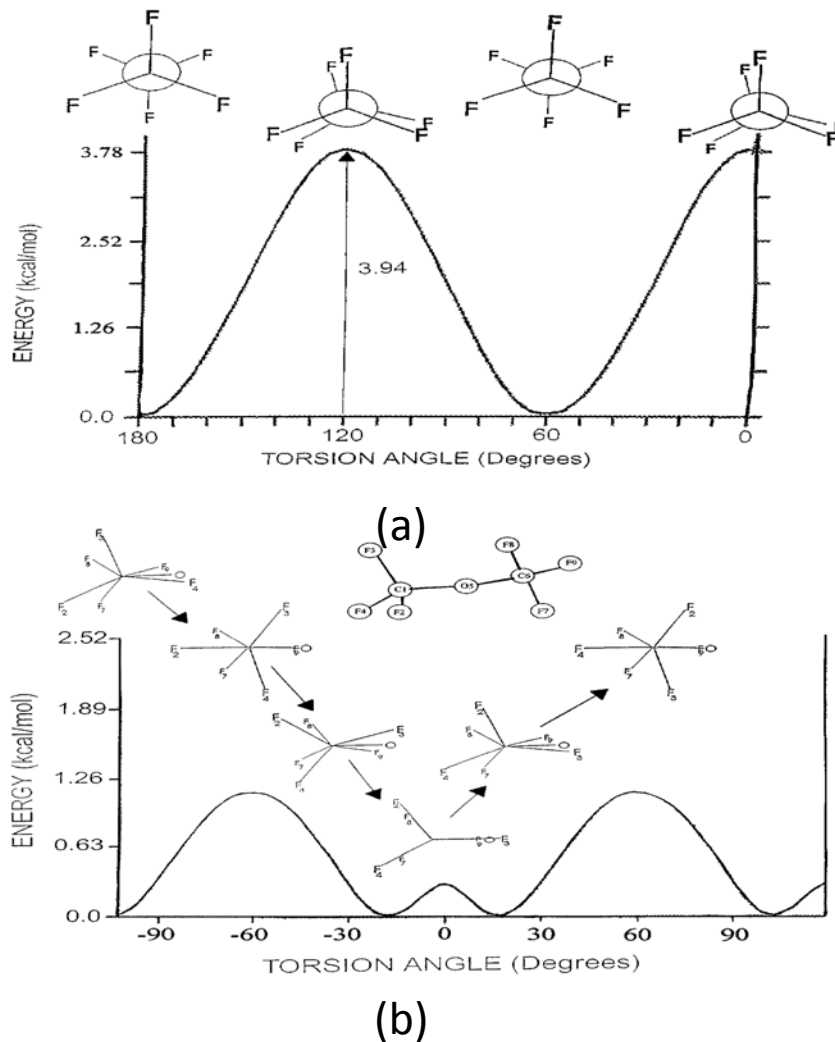


Figure 26. (a) Torsional potential for the perfluoroethane C-C bond and (b) torsional potential for the perfluoroethane C-O bond.²⁷ (Springer and Tribology letters, 7, 1999, 91, Impact of polymer structure and confinement on the kinetics of Zdol 4000 bonding to amorphous-hydrogenated carbon, Waltman, R. J.; Tyndall, G. W.; Pacansky, J.; Berry, R. J. figure (6), (7), Copyright © 1999, with kind permission from Springer Science and Business Media)

Therefore, the overall rigidity of CLP is expected to be higher than Zdol since it contains more C-C bond, More importantly, if considering the steric effect, which results from the side chains, to the rotational energy barrier of C-C bond in CLP, the rotational energy barriers of C-C bonds in CLPs backbone should be even larger. As shown before in Figure 2, ZDOL is a single perfluoropolyether chain with two hydroxyl functional groups on termini, while CLPs have either

pentafluoro (-CH₂CF₂CF₃) or trifluoro (-CH₂CF₃) side combs attached to carbon atoms in C-C bond. Due to the existence of bulky side combs, free rotation for C-C should be much harder than Zdol, which has no side groups attached to their C-C/C-O bonds. In Daley's organic chemistry book, he stated that the larger the substitute group on a molecule, the closer that group will be to another group on an adjacent carbon, consequently the barrier to free rotation increases.²⁸ In other words, if there is no substitute group attached to a backbone, an enormous variety of chain conformation can be realized through rotations of C-C single bonds joining successive chain atoms; however, if there are large substitutes attached to the center atoms of backbone, the number of conformation is greatly reduced due to the steric hindrance of bulky substitutes.²⁸ It has also been proved experimentally that rotation about single C-C bond between sp² and sp³ hybridized carbon atoms can be hindered by bulky substitutes.²⁹ For example, the internal rotational energy barrier of C-C bond in ethane is about 2.9kcal/mol, while that of butane, which can be considered as obtained from substituting one hydrogen with a methyl group on each carbon atom of ethane, is 5.2kcal/mol, which is nearly twice as big as ethane.³⁰ In addition, in biphenyl derivatives, when one hydrogen atom is substituted by -CH₃ group in each benzene ring, the rotational energy barrier of C-C bond is 17.4kcal/mol, if, methyl group is replaced by a larger group like -CH(CH₃)₂, rotational energy barrier becomes greater than 26.1kcal/mol.²⁹ Based on these previous results, it is clear that adding side groups will increase the free rotational energy barrier of C-C single bond via steric hindrance effect to a great extent.

All in all, CLPs molecules are more rigid than Zdol due to the effect of both the C-C bond numerically dominating the CLP backbone, which results in more "hindered rotation" bonds, and bulky side chains on CLPs, which further increases the free rotational energy barrier

in a magnificent manner. Therefore, a more rigid conformation of CLPs lubricant-thin film is understandable from the view of steric effect.

Another significant difference between ZDOL and CLPs is the chemical composition of backbone, which could be a second reason resulting in a conformation difference. The backbone of ZDOL is fluorocarbon while that of CLPs is hydrocarbon. Gellman et al. have proposed an electron donation mechanism between electron lone pairs of oxygen atom from an ether bond in lubricant and the amorphous hydrocarbon (α -CH) overcoat film on media surface to explain their finding that a decrease of hydrogen content in α -CH film results in an increase in heat of adsorption of lubricants.¹ If bonding occurs by electron donation from oxygen lone pair to the α -CH film, then an increase in the electron affinity of the film will increase the bond strength. Hydrogen is electropositive with respect to carbon, so removal of hydrogen from the film effectively increases the electron affinity of the film.¹ This proposed interaction could be another major interaction between polymers and carbon surface in addition to hydrogen bonding interaction between polar end group of polymer and active bonding sites of carbon surface.¹⁴ If this proposed mechanism is true, electron donation mechanism might involved in the lubricant/silicon wafer substrate system as well due to the same type of donor-acceptor interaction. It is worth noting that electron donation will be weakened with the existence of another strongly electronegative atom like fluorine in the lubricant film because it will decrease the electron density around oxygen atom due to its' ability to attract lone electrons.¹ (see Figure 27)

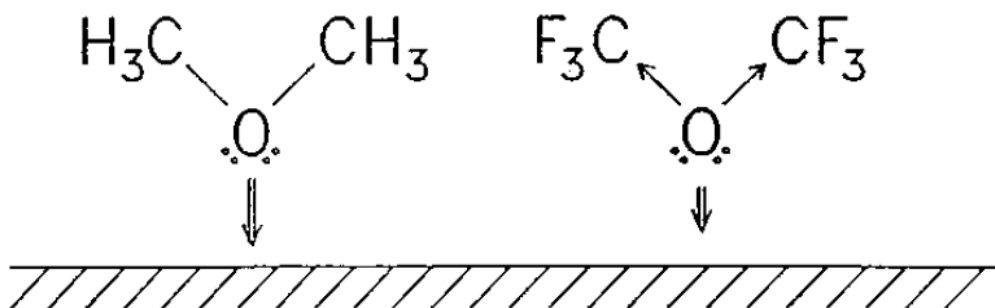


Figure 27. Schematic description of electron donation mechanism.¹ (Reprinted with permission from Cornaglia, L.; Gelman, A. J. *Journal of Vacuum Science & Technology A* 1997, 15, 2755. Copyright © 1997, American Vacuum Society)

Therefore, by considering there is no fluorine atom in the backbone of CLPs, the electron donation would be better established compared to ZDOL, which could result in a stronger electron donation interaction, and thus leads to a stronger polymer-solid attraction and flatter molecular conformation.

Whether flat or oblate is an indication of backbone behavior of polymer molecules, since CLPs also have side combs, what will the orientation of those combs? Answers to this question can be obtained from the monolayer thickness comparisons between PF-636 and PF-656 or PF-6320 and PF-6520 because the only difference between them is the side chain length. From Table 12, monolayer thickness of PF-656, 0.64 ± 0.04 nm, is larger than that of PF-636, which is 0.48 ± 0.02 nm, while monolayer thickness of PF-6520, 0.80 ± 0.06 nm is larger than that of PF-6320, which is 0.69 ± 0.05 nm. Since the side chain length of PF-65X is longer than that of PF-63X, while the backbones are exactly the same, it is reasonable to conclude that side combs of CLPs are more or less oriented towards the film-air interface and away from the carbon surface. Rough estimations of side comb lengths of both PF-63X and PF-65X were made based

on bond angle and bond length calculations. Since C-C, C-F and C-O bond angles are all around 120° , the monolayer thickness differences of CLPs as shown in Table 12. That is to say, our side chain length estimation results further suggest our hypothetical conformation that side combs tend to face towards lubricant-air interface while backbone lays relatively flat on the substrate. Such a side comb orientation can be explained from the surface energy point of view. Since the combs have lower surface energy due to strong electronegativity of fluorine atoms, they will try to find their way to get out of the bulky lubricant film to minimize the overall surface energy.

In conclusion, the conformations of ZDOL lubricants on silicon wafer substrate are oblate-like random coils close to the conformation of polymer in good solvent that corresponds to a molecular weight exponent of 0.6; while the conformations of new developed disk lubricant CLPs are more rigid and flatter, which corresponds to a molecular weight exponent of around 0.2 to 0.3. A proposed schematic conformation picture of ZDOL and CLPs is shown below in Figure 28.

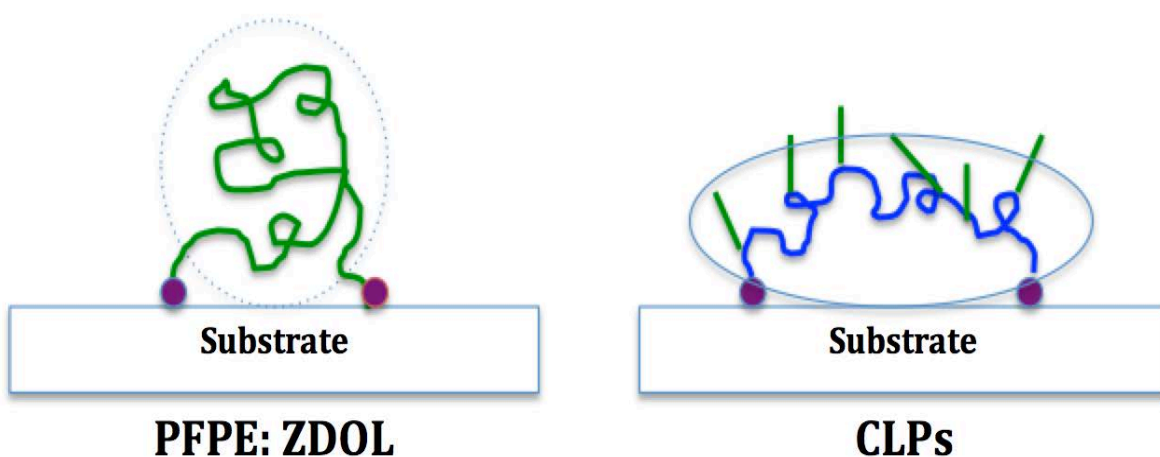


Figure 28. Schematic ZDOL and CLPs conformation based on current thesis results.

5.3 ADSORPTION KINETICS

In addition to using molecular weight exponent n to explore the conformation of ZDOL and CLPs after adsorption onto silicon wafer surface, it is also possible to investigate conformation difference between ZDOL and CLPs from adsorption kinetics point of view (see Figure 29), which serves as a secondary support here to elucidate their conformations.

It is important to point out that in this thesis we studied the correlation between adsorbed bonded lubricant film thickness and molar concentration of polymer solution instead of between film thickness and dwell time by setting the dwell time as a constant. It is understandable if one polymer reached saturated adsorption status at a lower molar concentration, it adsorbs faster as well by considering the adsorption time is consistent. Based on kinetics profiles of different polymer shown in Figure 29, it is clear that bonded thicknesses of ZDOL plateau at much higher concentration compared to CLPs. For both ZDOL 2000 and ZDOL 4000, we cannot determine the mole concentration corresponding to saturated bonded thickness. A trend shown for ZDOL 2000 is that the increasing trend slowed down a little bit at a mole concentration of around 0.0002 mol/L, while for ZDOL 4000, bonded layer thickness increases faster and faster as concentration increases. The trend difference between ZDOL 2000 and ZDOL 4000 is understandable if considering the backbone size of ZDOL 4000 is nearly twice as large as ZDOL 2000. Based on previous discussion, our monolayer thicknesses and molecular weight exponent results suggest that the conformation of ZDOL film is oblate-like slightly stretched random coil, thus a larger chain confined within a similar space might make the interior structure more complex and bulky; as a result, it should be harder for the end groups to get exposed and find the appropriate bonding site on silicon wafer surface to form hydrogen bonding.

Therefore, ZDOL 2000 should be easier to bond to silicon surface than ZDOL 4000; put it another way, bonded thickness of ZDOL 2000 should saturate at lower concentration than ZDOL 4000, which is consistent with our kinetics results. For CLPs, since the backbone is more rigid than ZDOL, and polar groups locate at two terminals of the backbone, we hypothesize that polar end groups might have a much better chance to be exposed, which could leads to easier access of finding bonding sites on silicon wafer surface and faster adsorption. As shown in Figure 29, bonded thicknesses of CLPs saturated at around 0.0003mol/L, compared to the saturation concentration of ZDOL, which is not even reflected, it is obvious that adsorption process of CLPs is much faster than ZDOL.

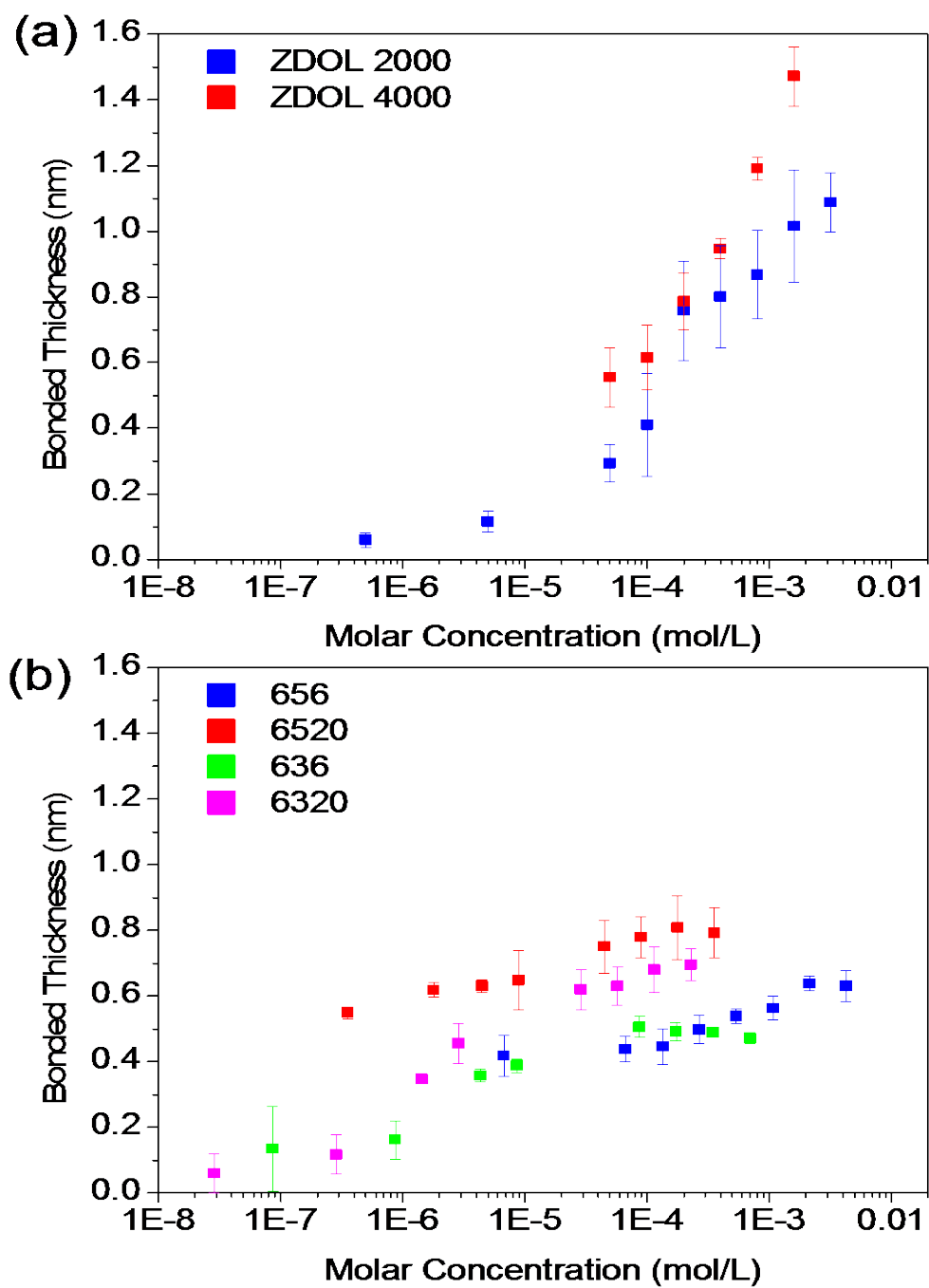


Figure 29. (a) Adsorption profile of ZDOL as a function of molar concentration (b) Adsorption profile of CLPs as a function of molar concentration. (All experiments are based on 30 min dwell time)

Last but not least, since CLPs thicknesses saturated at lower concentration compared to ZDOL with a same dwell time, if considering industrial fabrication, the amount of CLPs required to fabricate a complete lubricant film is much smaller than the amount of ZDOL required. On account of that, CLPs have higher cost efficiency than ZDOL besides lower cost as mentioned before as well.

To summarize, our kinetics results further supported our conclusions that ZDOL forms oblate conformation after adsorption onto silicon wafer while conformations of CLPs are more rigid and flatter.

6.0 CONCLUSION

Nanofilm conformation of commercially used hard disk drive lubricant ZDOL2000 and ZDOL4000, as well as a series of novel lubricants called comb-like polymers were investigated via analysis of molecular weight exponent n , which requires the determination of monolayer thickness. A new method named as saturated bonding adsorption here was applied to explore the monolayer thicknesses of interested lubricants.

Monolayer thicknesses of ZDOL2000 and ZDOL4000 were measure to be 1.02 ± 0.01 nm and 1.59 ± 0.21 nm, respectively, which were lower than previously reported monolayer thicknesses based on different methodologies, e.g. surface energy measurement, spreading, etc. The difference has been attributed to the fact that the monolayer thickness is taken as the bonded layer in the current thesis while in previous studies, total layer combined both bonded and mobile fraction was taken as the monolayer thickness. The molecular weight exponent n of ZDOL was calculated to be 0.64 ± 0.06 , which is close to a theoretically derived exponent of 0.6, which corresponds to polymer chains conformation in good solvent.

Monolayer thicknesses of PF-636, PF-6320, PF-656, and PF-6520 were measured to be 0.48 ± 0.02 nm, 0.69 ± 0.05 nm, 0.64 ± 0.04 nm, and 0.80 ± 0.06 nm, respectively; and resulted n values of PF-63X and PF-65X are 0.33 ± 0.04 and 0.20 ± 0.01 , which indicates a more rigid and flatter conformation compared to ZDOL. The difference in the conformation between

CLPs and Zdol has been attributed to the different chain rigidity: the large side groups in CLP increases rotational energy barrier of C-C bond and thus render the chain more rigid. This conclusion was further supported by our kinetics data. In addition, the monolayer thicknesses of CLPs turned out to be significantly smaller than ZDOL, which indicates that CLPs have the potential to substitute ZDOL as the new hard disk lubricant though further characterizations of CLPs are required.

APPENDIX A

Table 14. Water contact angle and hexadecane contact angle measurements of PF-636.

Concentration (g/L)	WCA					HCA				
	Trial 1	Trial 2	Trial 3	Average	Std	Trial 1	Trial 2	Trial 3	Average	Std
6.4	41.4	41.4	41.0	41.3	0.2	19.6	17.9	21.0	19.5	1.6
3.2	43.1	42.5	43.6	43.1	0.6	25.7	24.7	27.1	25.8	1.2
1.6	43.4	43.7	43.3	43.5	0.2	26.4	28.3	25.9	26.9	1.3
0.8	41.7	41.6	40.8	41.4	0.5	29.3	27.5	27.7	28.2	1.0
0.4	41.3	41.4	41.7	41.5	0.2	30.5	31.7	29.7	30.6	1.0
0.2	34.5	35.8	37.3	35.9	1.4	31.6	31.7	33.5	32.3	1.1
0.1	34.6	34.9	35.9	35.1	0.7	30.5	31.5	31.6	31.2	0.6
0.01	22.4	22.8	23.8	23.0	0.7	33.6	33.6	35.7	34.3	1.2
0.001	17.8	19.8	20.5	19.4	1.4	33.9	35.2	35.2	34.8	0.8
0.0001	19.1	22.7	23.7	21.8	2.4	38.0	41.3	42.8	40.7	2.5
0.0001(5min)	19.6	20.8	20.1	20.2	0.6	39.5	41.2	43.2	41.3	1.9
0.0001(no dwell)	10.7	12.1	12.2	11.7	0.8	31.1	33.2	38.1	34.1	3.6
0.001(no dwell)	10.1	10.8	11.3	10.7	0.6	26.6	27.7	31.3	28.5	2.5
0.005(no dwell)	27.2	29.2	29.6	28.7	1.3	29.9	31.6	32.0	31.2	1.1
0.01(no dwell)	10.2	12.8	15.6	12.9	2.7	30.3	31.3	32.0	31.2	0.9
0.1(no dwell)	19.9	20.2	21.5	20.5	0.9	32.5	33.5	34.0	33.3	0.8
0.2(no dwell)	19.7	19.9	20.3	20.0	0.3	31.0	31.3	34.4	32.2	1.9
0.4(no dwell)	25.0	25.8	27.7	26.2	1.4	30.4	31.3	32.2	31.3	0.9
0.8(no dwell)	32.7	33.3	35.8	33.9	1.6	26.9	26.4	26.2	26.5	0.4

*Run#1, concentrations with no dwell time specification corresponds to 30 min dwell

Table 15. Water contact angle and hexadecane contact angle measurements of PF-636.

Concentration (g/L)	WCA					HCA				
	Trial 1	Trial 2	Trial 3	Average	Std	Trial 1	Trial 2	Trial 3	Average	Std
0.0001	24.1	25.9	28.4	26.1	2.2	31.3	32.4	33.8	32.5	1.3
0.001	20.5	20.6	23.2	21.4	1.5	24.9	25.1	27.3	25.8	1.3
0.005	24.4	26.0	26.8	25.7	1.2	30.8	32.0	32.6	31.8	0.9
0.01	18.7	19.0	19.4	19.0	0.4	28.8	29.9	30.8	29.8	1.0
0.1	8.7	9.5	10.1	9.4	0.7	29.7	30.8	31.9	30.8	1.1
0.2	12.1	12.9	13.5	12.8	0.7	30.0	30.6	33.0	31.2	1.6
0.4	15.0	16.5	16.7	16.1	0.9	29.8	31.5	32.7	31.3	1.5
0.8	13.1	17.0	18.3	16.1	2.7	30.9	31.3	32.1	31.4	0.6

* Run#2, dwell time = 0 min

Table 16. Water contact angle and hexadecane contact angle measurements of PF-636.

Concentration (g/L)	WCA					HCA				
	Trial 1	Trial 2	Trial 3	Average	Std	Trial 1	Trial 2	Trial 3	Average	Std
0.0001	12.3	13.1	17.2	14.2	2.6	14.0	15.0	18.5	15.8	2.4
0.001	9.5	10.6	13.5	11.2	2.1	19.1	22.2	24.0	21.8	2.5
0.005	9.9	10.5	12.6	11.0	1.4	31.6	31.7	33.4	32.2	1.0
0.01	11.0	12.0	12.7	11.9	0.9	31.0	31.9	32.0	31.6	0.6
0.1	16.6	17.1	17.3	17.0	0.4	33.1	33.3	33.5	33.3	0.2
0.2	18.9	22.7	23.1	21.6	2.3	31.0	31.3	31.6	31.3	0.3
0.4	28.3	28.6	32.5	29.8	2.3	29.8	30.8	31.4	30.7	0.8
0.8	17.7	17.9	19.0	18.2	0.7	32.0	33.8	34.0	33.3	1.1

*Run#3, dwell time = 0 min

Table 17. Water contact angle and hexadecane contact angle measurements of PF-636.

Concentration (g/L)	WCA					HCA				
	Trial 1	Trial 2	Trial 3	Average	Std	Trial 1	Trial 2	Trial 3	Average	Std
0.0001	6.2	6.4	6.7	6.4	0.3	10.8	10.9	11.0	10.9	0.1
0.001	8.1	8.9	8.5	8.5	0.4	20.8	21.5	22.8	21.7	1.0
0.005	12.2	13.4	15.1	13.6	1.5	29.6	29.7	29.7	29.7	0.1
0.01	16.2	17.0	18.6	17.3	1.2	30.2	31.1	32.6	31.3	1.2
0.1	18.3	18.7	18.9	18.6	0.3	32.7	33.4	34.7	33.6	1.0
0.2	16.9	19.3	20.8	19.0	2.0	32.8	32.9	33.1	32.9	0.2
0.4	15.9	17.0	18.8	17.2	1.5	30.2	32.0	33.5	31.9	1.7
0.8	17.7	20.2	22.7	20.2	2.5	32.4	30.7	34.0	32.4	1.7

*Run#4, dwell time = 0 min

Table 18. Water contact angle and hexadecane contact angle measurements of PF-636.

Concentration (g/L)	WCA					HCA				
	Trial 1	Trial 2	Trial 3	Average	Std	Trial 1	Trial 2	Trial 3	Average	Std
0.0001	5.0	5.6	3.0	4.5	1.4	12.0	12.4	13.0	12.5	0.5
0.001	4.0	6.1	6.2	5.4	1.2	10.1	19.3	21.5	17.0	6.0
0.005	9.2	9.5	9.7	9.5	0.3	30.3	30.9	34.0	31.7	2.0
0.01	15.2	15.5	17.0	15.9	1.0	31.2	33.3	34.6	33.0	1.7
0.1	13.2	13.2	15.1	13.8	1.1	33.4	33.6	34.5	33.8	0.6
0.2	15.9	16.3	17.0	16.4	0.6	33.3	33.9	36.3	34.5	1.6
0.4	16.0	16.7	18.4	17.0	1.2	32.7	33.7	35.3	33.9	1.3
0.8	17.0	17.2	17.9	17.4	0.5	30.2	30.5	33.6	31.4	1.9

*Run#5, dwell time = 0 min

Table 19. Water contact angle and hexadecane contact angle measurements of PF-636.

Concentration (g/L)	WCA					HCA				
	Trial 1	Trial 2	Trial 3	Average	Std	Trial 1	Trial 2	Trial 3	Average	Std
0.0001	4.0	4.2	4.5	4.2	0.3	6.7	7.2	8.0	7.3	0.7
0.001	2.8	3.0	4.6	3.5	1.0	11.8	13.1	10.6	11.8	1.3
0.005	8.9	10.0	12.7	10.5	2.0	31.9	32.4	33.5	32.6	0.8
0.01	10.7	11.5	12.4	11.5	0.9	34.4	34.9	36.6	35.3	1.2
0.1	17.6	18.0	19.4	18.3	0.9	37.1	37.3	38.8	37.7	0.9
0.2	18.2	19.5	19.8	19.2	0.9	35.3	36.9	37.3	36.5	1.1
0.4	22.8	23.3	24.6	23.6	0.9	36.7	37.5	40.7	38.3	2.1
0.8	42.5	42.6	42.8	42.6	0.2	34.5	34.7	37.6	35.6	1.7

*Run#1, dwell time = 0 min

Table 20. Water contact angle and hexadecane contact angle measurements of PF-636.

Concentration (g/L)	WCA					HCA				
	Trial 1	Trial 2	Trial 3	Average	Std	Trial 1	Trial 2	Trial 3	Average	Std
0.0001	14.2	17.3	18.4	16.6	2.2	10.6	12.3	14.9	12.6	2.2
0.001	8.0	8.6	8.8	8.5	0.4	8.6	10.4	11.0	10.0	1.2
0.005	15.1	15.5	16.3	15.6	0.6	29.0	31.4	31.4	30.6	1.4
0.01	14.2	15.2	15.9	15.1	0.9	35.6	36.1	36.7	36.1	0.6
0.1	22.7	23.4	24.3	23.5	0.8	37.1	38.0	39.3	38.1	1.1
0.2	28.4	29.9	30.1	29.5	0.9	30.9	34.7	36.0	33.9	2.7
0.4	29.0	29.0	29.8	29.3	0.5	34.6	37.1	38.0	36.6	1.8
0.8	42.3	42.9	44.5	43.2	1.1	36.1	36.4	36.6	36.4	0.3

*Run#2, dwell time = 0 min

Table 21. Water contact angle and hexadecane contact angle measurements of PF-636.

Concentration (g/L)	WCA					HCA				
	Trial 1	Trial 2	Trial 3	Average	Std	Trial 1	Trial 2	Trial 3	Average	Std
0.0001	5.2	5.6	5.8	5.5	0.3	6.9	9.6	9.9	8.8	1.7
0.001	8.4	12.2	12.8	11.1	2.4	12.9	15.0	16.7	14.9	1.9
0.005	18.8	19.3	19.9	19.3	0.6	23.3	23.7	30.9	26.0	4.3
0.01	14.8	15.1	15.5	15.1	0.4	28.4	29.0	29.6	29.0	0.6
0.1	17.6	19.0	19.1	18.6	0.8	35.8	36.6	38.5	37.0	1.4
0.2	18.3	20.0	21.4	19.9	1.6	35.8	35.9	36.7	36.1	0.5
0.4	22.9	24.9	25.5	24.4	1.4	35.5	37.6	37.9	37.0	1.3
0.8	29.9	32.0	34.1	32.0	2.1	35.8	35.9	36.3	36.0	0.3

*Run#3, dwell time = 0 min

Table 22. Water contact angle and hexadecane contact angle measurements of PF-636.

Concentration (g/L)	WCA					HCA				
	Trial 1	Trial 2	Trial 3	Average	Std	Trial 1	Trial 2	Trial 3	Average	Std
0.0001	7.3	7.4	8.0	7.6	0.4	8.6	10.4	11.0	10.0	1.2
0.001	12.1	12.9	13.4	12.8	0.7	10.7	12.4	15.3	12.8	2.3
0.005	10.3	13.0	11.7	11.7	1.4	22.0	24.2	26.0	24.1	2.0
0.01	15.5	16.3	17.6	16.5	1.1	24.0	25.0	25.6	24.9	0.8
0.1	20.5	21.8	23.0	21.8	1.3	27.8	28.9	29.9	28.9	1.1
0.2	23.9	24.2	26.7	24.9	1.5	29.9	30.7	35.2	31.9	2.9
0.4	29.2	29.3	32.4	30.3	1.8	30.9	31.4	32.4	31.6	0.8
0.8	41.5	43.4	45.2	43.4	1.9	31.0	31.1	31.9	31.3	0.5

*Run#4, dwell time = 0 min

Table 23. Water contact angle and hexadecane contact angle measurements of PF-636.

Concentration (g/L)	WCA					HCA				
	Trial 1	Trial 2	Trial 3	Average	Std	Trial 1	Trial 2	Trial 3	Average	Std
0.0001	5.1	6.6	8.3	6.7	1.6	10.5	11.0	11.2	10.9	0.4
0.001	8.5	11.0	11.2	10.2	1.5	11.6	12.5	16.0	13.4	2.3
0.005	13.6	14.1	15.6	14.4	1.0	27.5	29.5	30.6	29.2	1.6
0.01	17.0	17.1	17.6	17.2	0.3	25.6	26.4	27.4	26.5	0.9
0.1	23.6	25.0	27.2	25.3	1.8	28.5	28.7	29.9	29.0	0.8
0.2	26.0	30.4	32.2	29.5	3.2	27.8	30.1	30.4	29.4	1.4
0.4	39.0	40.3	40.4	39.9	0.8	29.6	30.5	32.1	30.7	1.3
0.8	43.1	45.7	46.0	44.9	1.6	29.7	31.5	34.2	31.8	2.3

*Run#5, dwell time = 0 min

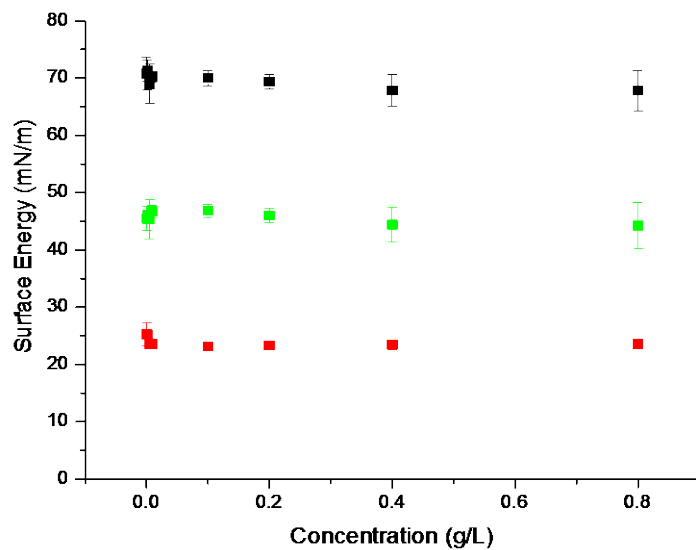


Figure 30. Surface energy profile of PF-636. Black symbols correspond to total surface energy, green symbols correspond to polar surface energy, and red symbols correspond to dispersive surface energy.

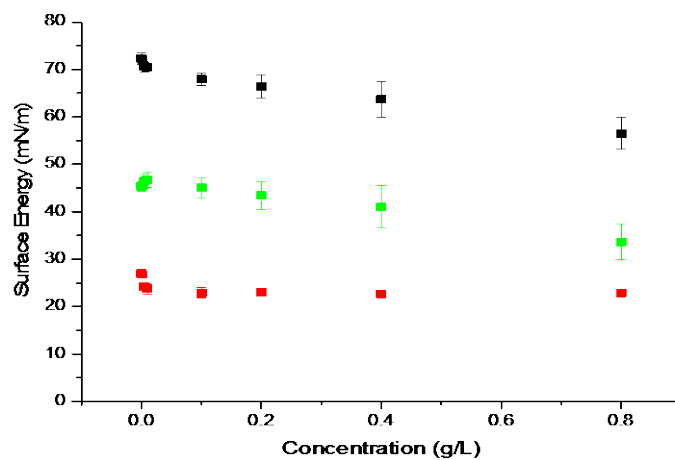


Figure 31. Surface energy profile of PF-6320. Black symbols correspond to total surface energy, green symbols correspond to polar surface energy, and red symbols correspond to dispersive surface energy.

BIBLIOGRAPHY

- (1) Cornaglia, L.; Gellman, A. J. *Journal of Vacuum Science & Technology A* **1997**, *15*, 2755.
- (2) Gui, J. *IEEE Transactions on Magnetics* **2003**, *39*, 716.
- (3) Hsia, Y.-T.; Guo, Q.; Izumisawa, S.; Jhon, M. *Microsystem Technologies* **2005**, *11*, 881.
- (4) Ellis, D. A.; Martin, J. W.; De Silva, A. O.; Mabury, S. A.; Hurley, M. D.; Sulbaek Andersen, M. P.; Wallington, T. J. *Environmental Science & Technology* **2004**, *38*, 3316.
- (5) Young, C. J.; Hurley, M. D.; Wallington, T. J.; Mabury, S. A. *Environmental Science & Technology* **2006**, *40*, 2242.
- (6) Kasai, P. H.; Wheeler, P. *Applied Surface Science* **1991**, *52*, 91.
- (7) Kasai, P. H.; Raman, V. *Tribology Letters* **2004**, *16*, 29.
- (8) Li, L.; Jones, P. M.; Merzlikine, A. G.; Hsia, Y. T. *Tribology Letters* **2004**, *17*, 953.
- (9) Guo, Q.; Li, L.; Hsia, Y.-T.; Jhon, M. S. *IEEE Transactions on Magnetics* **2006**, *42*, 2528.
- (10) Ma, X.; Gui, J.; Smoliar, L.; Grannen, K.; Marchon, B.; Jhon, M. S.; Bauer, C. L. *The Journal of Chemical Physics* **1999**, *110*, 3129.
- (11) Tyndall, G. W.; Waltman, R. J.; Pocker, D. J. *Langmuir* **1998**, *14*, 7527.
- (12) Marchon, B. In *Tribology Series*; D. Dowson, M. P. G. D., Lubrecht, A. A., Eds.; Elsevier: 2002; Vol. Volume 40, p 217.
- (13) Guo, Q.; Li, L.; Hsia, Y.-T.; Jhon, M. S. *Journal of Applied Physics* **2005**, *97*, 10P302.

- (14) Ma, X.; Gui, J.; Grannen, K.; Smoliar, L.; Marchon, B.; Jhon, M.; Bauer, C. *Tribology Letters* **1999**, *6*, 9.
- (15) Chen, H.; Guo, Q.; Jhon, M. S. *IEEE Transactions on Magnetics* **2007**, *43*, 2247.
- (16) Karplus, M. A.; Waltman, R. J.; Pocker, D. J. *Journal of Applied Physics* **2000**, *87*, 6161.
- (17) Mayeed, M. S.; Kato, T. In *Magnetic Recording Conference, 2002. Digest of the Asia-Pacific 2002*, p BP4.
- (18) Vig, J. In *Surface Contamination*; Mittal, K. L., Ed.; Springer US: 1979, p 235.
- (19) Merzlikine, A. G.; Li, L.; Jones, P.; Hsia, Y.-T. *Tribology Letters* **2005**, *18*, 279.
- (20) Wang, Y.; Sun, J.; Li, L. *Langmuir* **2012**, *28*, 6151.
- (21) Jung, J.; Bork, J.; Holmgaard, T.; Anker Kortbek, N. *Ellipsometry* **2004**.
- (22) Kattner, J.; Hoffmann, H. *The Journal of Physical Chemistry B* **2002**, *106*, 9723.
- (23) Gennes, P.-G. d. *Scaling Concepts in Polymer Physics*; Cornell University Press
- (24) Enders S, L. K., Schrader P, Zeiner T. *Polymers* **2012**, *4*, 72.
- (25) Flory, P. *Principles of Polymer Chemistry*; Cornell University Press: Ithaca, N.Y., 1953
- (26) rkt.chem.ox.ac.uk/lectures/liqsolns/polymer_solutions.html
- (27) Waltman, R. J.; Tyndall, G. W.; Pacansky, J.; Berry, R. J. *Tribology Letters* **1999**, *7*, 91.
- (28) Richard F. Daley, S. J. D. *Organic Chemistry*; Daley & Daley, 2005 131.
- (29) Kessler, H. *Angewandte Chemie International Edition in English* **1970**, *9*, 219.
- (30) Mo, Y. *Wiley Interdisciplinary Reviews: Computational Molecular Science* **2011**, *1*, 164.